SUPPLEMENTAL

A. Detailed Technical Discussions

a. Model Development and Justification

Antibodies and antibody fragments are promising agents for cancer detection and treatment. There are currently 12 Food and Drug Administration (FDA)-approved antibody drugs for cancer, 8 more in phase III clinical trials, and dozens in phase I and II clinical trials(*1, 2*). Despite this progress, there are still significant challenges limiting the full potential of these drugs. This model addresses some of these issues.

Targeting tumor tissue with antibodies is a complex task with many barriers (*3-5*). Poor transport in tumors can place severe pharmacokinetic restrictions on anti-tumor antibodies, and the large mass of these molecules exacerbates these effects for this class of drug. Treating cancer requires targeting both avascular micrometastases and vascularized tumors, and these two settings have significantly different pharmacokinetic properties.

Antibody delivery to micrometastases requires transport across healthy capillaries into normal tissue surrounding the metastasis, then diffusion into the mass of tumor cells. Lymphatics constantly drain normal tissue, and extravasation decreases as plasma antibody concentration drops for bolus doses. Antibodies diffuse into the tumor spheroid and bind free antigen, depleting the pool of free antibody and therefore slowing penetration(*5*). Once bound, the antibody/antigen complex is generally taken up into the cell either by specific endocytosis of the receptor/antigen, or through normal turnover of the cell surface(*6, 7*). Antibody that is not recycled to the surface is directed to lysosomes where it is catabolized(*8*).

Targeting of vascularized tumors is similar, but with key differences. There is no normal tissue compartment following extravasation, and transport occurs across the walls of the tumor vasculature, rather than across the walls of surrounding healthy capillaries. In general, tumor blood vessels have much higher permeabilities, larger diameters, and more tortuous paths; however, these properties are heterogeneous throughout the tumor(*9*). Higher permeabilities along with the absence of functional lymphatics cause an increase in interstitial pressure(*10*). Whereas convection is mainly responsible for extravasation in healthy tissue, diffusion is the dominant mode in most of a vascularized tumor, due to the relatively uniform elevated interstitial pressure within the tumor.

All significant rate processes must be captured in the kinetic model, including local and systemic clearance, extravasation, convection and diffusion, binding, release, endocytosis, recycling, and

degradation. The endocytosis rate is particularly emphasized in this analysis since antibody internalization can be significant(*6, 7, 11-17*), and due to internalization, antibody concentration does not simply build up within the tumor tissue until all binding sites are occupied. The various rates that dictate the outcome are more complicated than this.

Despite the complexity inherent in the problem, there are characteristic, measurable rates present in both scenarios. By examining the different pharmacokinetic steps, predictions can be made on the level of targeting in both cases. *In vitro,* Murphy and colleagues examined internalization and diffusion of immunotoxins in isolated cell spheroids (*18*). Their analysis of the effects of cellular trafficking in spheroids provides insight into targeting micrometastases *in vivo*. Rippley and Stokes have analyzed internalization and trafficking in tissue using transferrin as a model(*19*). Adams and colleagues have shown that high affinity antibodies do not penetrate more than a few cell diameters in mouse xenografts, even after 24 hours with a 100 μg bolus dose of scFv in a nephrectomized animal, eliminating rapid renal clearance of these fragments (*20*). Lower affinity antibodies, however, fully penetrated the tissue.

This paper uses numerical simulation to examine the model system and discussed some of the trade-offs between efficacy and distribution for internalized drugs. The kinetics of both high and low affinity antibodies can be numerically simulated, but high affinity antibodies were chosen for this analysis. Association rates for both high and low affinity antibodies are often similar. It is therefore due to lower affinity antibodies' faster off rates that they dissociate from antigen and penetrate faster into tumor tissue. Although extravasation, and therefore total tumor loading, of high and low affinity antibodies may be similar, the lower affinity antibodies are more homogeneously distributed. Unfortunately, the situation also works in reverse. Once antibody is cleared from the blood, the fast off rates of low affinity antibodies allow them to quickly dissociate and diffuse out of the tissue (*5*). No antibody retention at all can be observed for affinities of 100 nM or less (*20*). Even in a steady-state scenario, all other things being equal, lower affinity antibodies have a lower tumor-normal tissue ratio. Higher affinity antibodies saturate tissue and are retained much longer, although their distribution prior to saturation is heterogeneous, since they saturate antigen closer to the antibody source before moving deeper into tissue (*5, 21*).

The objective of this modeling exercise is to derive dimensionless parameters that characterize the relative rates of the most significant kinetic processes in tumor penetration. Model development involved the consideration of numerous issues. A simplified diffusion-only spherical geometry for micrometastases and cylindrical geometry around capillaries in vascularized tissues was used to model antibody penetration. Full numerical simulations of equations 7-14 were carried out in Matlab (The MathWorks) or simplified analytically.

For micrometastases, the model equations are identical to Graff et al. (*5*) The symmetry boundary condition used is the same, but the boundary condition at the edge of the metastasis is modified to account for the surrounding well mixed normal tissue. A biexponential plasma concentration is used in conjunction with flow in and out of the normal tissue:

$$[Ab]_{plasma}(t) = [Ab]_{plasma,0}\left(Ae^{-k_1 t} + Be^{-k_2 t}\right) \qquad 7.$$

where $[Ab]_{plasma,0}$ is the initial plasma concentration, A and B are the fraction of alpha and beta clearance, and k_1 and k_2 are the clearance rate constants for the alpha and beta phases. For the normal tissue:

$$\frac{d[Ab]_n}{dt} = \kappa[Ab]_{plasma}(t) - \lambda[Ab]_n(t) \qquad \text{initial condition: } [Ab]_n(0) = [Ab]_{n0} \qquad 8.$$

where λ is the lymphatic clearance rate, κ is the normal capillary transport rate, and $[Ab]_n$ is the interstitial normal tissue concentration.

The boundary condition is then:

$$(Ab)\big|_{r=R} = \varepsilon \cdot Ab_n \qquad 9.$$

Solid tumors are modeled using a two compartment model. With inside-out cylindrical geometry, the equations, similar to the micrometastasis, are:

$$\frac{\partial Ab}{\partial t} = D\frac{1}{r}\frac{\partial}{\partial r}\left(r\frac{\partial Ab}{\partial r}\right) - \frac{k_{on}}{\varepsilon}AbAg + k_{off}B \qquad 10.$$

$$\frac{\partial B}{\partial t} = \frac{k_{on}}{\varepsilon}AbAg - k_{off}B - k_eB \qquad 11.$$

$$\frac{\partial Ag}{\partial t} = R_s - \frac{k_{on}}{\varepsilon}AbAg + k_{off}B - k_eAg \qquad 12.$$

D is the diffusivity constant, r is the radius, k_{on}, k_{off}, and k_e are the binding, release, and endocytosis rate constants, R_s is the synthesis rate of free antigen, ε is the void fraction, and Ab, Ag, and B are the free antibody, free antigen, and bound antibody/antigen complex concentrations. Equation 10 shows that free antibody concentration changes due to diffusion, binding, and release of antibody. Bound antibody similarly changes due to binding and dissociation, but it also decreases due to internalization of the complex. Finally, free antigen is depleted or restored due to antibody binding and release, and it is also synthesized and internalized.

The boundary conditions are particularly important for the cylindrical model. The radius of each cylinder is similar to that of micrometastases due to oxygen diffusion limitations(*22, 23*). The condition used at the outer edge of the cylinder, away from the capillary, is a no flux, or mirror boundary condition (also non-interacting). At each point at the edge of the cylinder, it is imagined that that point is the outer edge of another cylinder around an adjacent capillary. Any free antibody at the edge of the cylinder will face an identical free antibody across the boundary, so there is no driving force for diffusion and thus no antibody crosses the barrier.

$$\left.\frac{\partial Ab}{\partial r}\right|_{r=R} = 0 \qquad 13.$$

The other boundary condition is at the radius of the inner cylinder, the capillary radius. This condition is more complex, and requires a mixed boundary condition (*9*).

$$-\frac{D}{P}\left(\frac{dAb}{dr}\right)\Bigg|_{r=R_{capillary}} + (Ab)\Big|_{r=R_{capillary}} = \varepsilon \cdot Ab_{plasma} \qquad 14a.$$

$$P\left(\left(\varepsilon[Ab]_{plasma}\right) - [Ab]\right) = -D\left(\frac{d[Ab]}{dr}\right) \qquad 14b.$$

Epsilon is necessary because antibody is going from the plasma into the tumor tissue, where the amount of accessible space is limited due to cellular volume and extracellular matrix. The flux of antibodies crossing the capillary is dependent both on the permeability of the capillary, P, and the rate at which extravasated antibodies diffuse. If there were no diffusion into the tissue, or the permeability was infinite, the concentrations would equilibrate across the capillary wall. The above equations were either solved numerically, using a Matlab program that implements the method of lines, or simplified and examined analytically.

Convection was explicitly ignored in the simulation of vascularized tumors(*24*). This is a conservative estimate, since convection across permeable tumor vessels carries antibody across the capillary barrier in the periphery of the tumor, where fluid leaks out of the vasculature and out the edges of

the tumor (*4, 10*). This is illustrated with drugs such as CEA-Scan, an imaging agent that often shows increased intensity at the tumor periphery (*25*). Convection therefore causes higher than expected levels of targeting at the periphery of tumors, which is more noticeable with small doses of antibody and low overall targeting. The small magnitude of convection in the tumor interior should not distort the symmetry around capillaries, justifying a one dimensional model (*26*).

Because general principles are sought here rather than a precise numerical description of a specific tumor geometry, this model comprises the simplest one dimensional description. Concentric cylinders represent the capillary surface on the inside and the edge of the volume of tissue targeted by that capillary on the outside, similar to that used by Fujimori et al.(*27*). The variable R represents the distance from the nearest capillary for the bulk tumor case and the distance from the micrometastasis center in that case. The stochastic nature of the tortuous vessels in solid tumors is too variable to make any general cases. Tumor vessels are fractal over smaller length scales (*22*), and larger tumors can have whole sections of tumor that completely lack functional vessels or have extremely high vascular density (*28*). Despite the differences in length scales, conservative estimates can be made based on experimental data. Highly vascularized areas will saturate more quickly, and free antibody from these regions will diffuse into more sparsely vascularized areas. The characteristic length will lie somewhere between the distances present in these extremes. Overall, the capillary surface area to tumor volume ratio (which can vary locally in a tumor) is the more important parameter that determines the appropriate length scale, and in the case for a small Biot number, results in a Thiele modulus normalized for the shape (*29*). This Krogh-like cylinder model has been criticized when used for tissue with less structured vessels. However, in this analysis we seek to capture characteristic rates that lead to saturation, not to mimic particular structures. For example, the Thiele modulus has been shown to be rather independent of geometry (*29*). Ultimately, the model will not describe large tumors with macroscale necrotic and avascular regions. However, for smaller tumors, on the scale of 1 cm used in xenograft studies and at the practical limit of detection for current non-invasive techniques in humans (*30-33*), conservative estimates should capture the necessary criteria for saturation.

Other features of vascular tumors not explicitly treated in the model include shedding, receptor/antigen down-regulation, intermittent blood flow, non-tumor cells, free antigen in the blood, and tissue heterogeneity. Shedding can be treated to a first approximation by using appropriate antigen concentrations. If the concentration of antigen increases in a tumor due to accumulation of shed antigen, the total antigen concentration would increase for initial saturation (clearance modulus, see below). As will be shown later, only the concentration of antigen still attached to cells would be relevant for internalizing antigen (see Thiele modulus analysis below). Large antigens such as CEA likely accumulate within the tumor given the lack of lymphatic drainage and poor capillary transport. Ultimately, the fate of the shed antigen would have to be considered for a more in-depth treatment. However, if not internalized (leading to antibody catabolism) shed antigen will actually favor penetration due to the lack of catabolic turnover. Similarly, down-regulation and/or large internal antigen levels can be treated using different effective concentrations. For down-regulation, the initial targeting will require saturation at the intrinsic surface antigen concentration. Once the tumor has initially been saturated, however, consumption will likely occur at the down-regulated concentration. This is important for drugs such as cetuximab, which has a high rate of internalization but down-regulates the total surface concentration (*34, 35*). As will be seen, the clearance modulus describes transient conditions for the initial saturation of antigen (most pertinent to rapidly clearing drugs), while the Thiele modulus describes a pseudo-steady state (often achieved with antibodies that persist in circulation). For internalization with recycling, if the internalization rate is rapid compared to penetration in the tissue, the initial saturation of the cells will include both the internal and external antigen fractions, so this is the relevant concentration. For catabolism, then, the degradation rate of internal antigen is the effective endocytosis rate. With slow internalization rates, only the cell surfaces become saturated early on, so this concentration is used for initial saturation. To maintain surface saturation, however, the consumption term is initially the internalization rate. Once the internal pool is saturated, this drops to the degradation rate of the antibody (supplemental section G). Hence, cellular trafficking can have a significant impact on the micropharmacokinetics (*36*).

Intermittent blood flow in tumor vessels is not explicitly treated. However, with the high concentrations of antibody in the plasma needed for saturation and low extravasation rates, depletion of plasma antibody is unlikely, even if blood flow periodically ceases in parts of the vessel. Typical time

scales for transient heterogeneity in flow are on the order of several minutes (*37, 38*). For antibodies that clear slower than this, the concentration profile would average out over time. However, rapidly cleared fragments, such as unmodified scFvs, could clear from the plasma before some periodically closed vessels open, causing greater heterogeneity and less uniformly effective targeting. For vessels that completely lack flow, extravasation is negligible, and the characteristic distance for adjacent vessels must be adjusted accordingly. Non-tumor cells, such as lymphocytes and fibroblasts, can be treated as antigen negative cells, and antibody will diffuse past them without binding, lowering the effective concentration. Although a concern, free antigen in the blood is typically several orders of magnitude lower than concentrations of antibody needed to saturate the tumor. This antigen would be complexed in the plasma, and cold dosing could be used to deplete this pool of antigen if needed (*39, 40*). Heterogeneities plague larger tumors, but given a high enough antibody concentration for saturation, the antibody will diffuse from areas of higher extravasation and/or lower antigen concentration to those areas with lower extravasation and/or higher antigen loads. Longer term effects, such as vascular remodeling and 'normalization' occur over longer time scales (*41*) and are beyond the scope of this paper.

b. Extended Model Results

The moduli are repeated below with some additional comments on the parameters.

Clearance Modulus

Vascularized Tumors

$$\Gamma_{tumor} \equiv \frac{\ln(2)\cdot R^2\left([Ag]/\varepsilon\right)}{2\cdot[Ab]_{plasma,0}\cdot P\cdot R_{cap}\left(A\cdot t_{1/2,\alpha}+B\cdot t_{1/2,\beta}\right)} = \frac{\text{Antibody saturation time}}{\text{Plasma clearance time (AUC)}}$$

The model can also incorporate cases where a constant infusion is given. This definition for the AUC is given later on in the supplemental. The ln(2) term is present since plasma half lives are used instead of rate constants, and the 2 in the denominator is leftover from the capillary area ($2\pi R_{cap}L$, where π and L, length, cancelled with the cylinder volume in the numerator). For most scenarios in solid tumors, the vessel wall provides the greatest resistance, which is why a diffusivity constant does not appear here. This dimensionless group is analogous to the simplification given by Baxter and Jain for an irreversibly bound, non-metabolized antibody(*42*).

Micrometastases

$$\Gamma_{met} \equiv \frac{R^2\left([Ag]/\varepsilon\right)}{6D\cdot\left(AUC_{Ab,normal}\right)} = \frac{\ln(2)\cdot R^2\left([Ag]/\varepsilon\right)}{6D\cdot\left([Ab]_{plasma,0}\left(\frac{K}{\lambda}\right)\left(A\cdot t_{1/2,\alpha}+B\cdot t_{1/2,\beta}\right)\right)}$$

Looking at the clearance modulus, it becomes apparent that for substantial uptake or saturation of solid tumors, a significant dose and slow clearance are necessary. Both of these contribute to secondary toxicity. Secondary toxicity can come from a variety of sources, such as antigen located in healthy tissue, non-specific dose to the bone marrow (which mimics that of the blood), and filtration by the liver and kidneys. Since antigen levels in healthy tissue are typically low for relevant antibodies, these sites become saturated quickly with large doses. Cold dosing can help block uptake in these more easily accessible sites. The dose to the bone marrow is close to that of the blood, so there is a direct trade between longer plasma half lives and larger doses to the bone marrow. Due to the poor transport in tumors, pretargeting methods may be required to target a large fraction of the tumor while sparing the bone marrow from large doses. Similarly with the liver and kidney, large doses cause these organs to filter a significant amount of antibody during binding of the tumor. Although blocking uptake of fragments to the kidney has helped lower this toxicity, pretargeting may be required to deliver a significant amount of radiation to a solid tumor while

avoiding renal complications. The fact that this is a late responding tissue means that researchers must design studies to examine effects several months after therapy.

Thiele Modulus

Vascularized Tumors

$$\phi_{tumor}^2 \equiv \frac{k_e R^2 \left({[Ag]}/{\varepsilon} \right)}{D \left(\frac{[Ab]_{plasma}}{1 + {1}/{Bi}} \right)} = \frac{\text{Antibody extravasation and diffusion time}}{\text{Antibody catabolism time}}$$

where $Bi \equiv \frac{2PR_{capillary}}{D} = \frac{\text{Extravasation rate}}{\text{Diffusion rate}}$

Using values from the literature, it can be seen that the Biot number is typically very small, even for tumor tissue with elevated permeability(*9*). For example, an IgG, D = 14 $\mu m^2/s$, extravasating from a 10 μm radius tumor capillary at a rate of $3x10^{-3}$ μm/s has a Biot number of $4x10^{-3}$. Similarly, an scFv has a Biot number around $1x10^{-3}$. Assuming a small Biot number, the Thiele modulus simplifies to a form similar to the clearance modulus.

Micrometastases

$$\phi_{met}^2 = \frac{k_e R^2 \left({[Ag]}/{\varepsilon} \right)}{D[Ab]_{n0}}$$

The normal tissue concentration is:

$$[Ab]_{n0} = \frac{\kappa}{\lambda}[Ab]_{plasma,0}$$

Technically, the Thiele modulus is a Damköhler number and was originally developed to characterize diffusion and reaction of chemicals in solid catalysts (*43*). The internalization rate constant will not be equal to the first-pass internalization rate of the antigen if the antibody is recycled (*44*), which is discussed later in the supplemental. [Ag] represents the concentration of antigen that is internalizing (which may be lower than the total concentration in the tumor if it is shed, sequestered, etc.). The product k_e[Ag] should be the total consumption rate of antibody in the tissue.

When examining the Thiele modulus, it is pertinent to mention that the concept of a "non-internalizing" antibody is very likely invalid for most membrane-bound antigens. Constitutive membrane turnover degrades most membrane proteins on the time scale of several hours (*45*, *46*), and this time scale is often similar to that for diffusion, as illustrated by the analyses here. As shown explicitly for trastuzumab(*44*), the appearance of non-internalization can result from efficient endocytic recycling, although even in this case the net antibody catabolism half life is ~6 hours. A more accurate description for apparently non-internalizing antibodies might be "efficiently recycled."

The capillary wall provides a significant barrier to transport, and this is present in both normal as well as tumor tissue. Although the permeability of healthy capillaries is lower than tumor vasculature, this effect is overshadowed by the increase in the surface area to tumor volume ratio and convection from lymphatic drainage compared to tumor tissue. A single micrometastasis is essentially fed by a multitude of capillaries in the surrounding normal tissue as they extravasate antibody into the interstitium. With large diffusivities (*47*) and relevant concentrations, transport outside the micrometastases is not limiting (*48*). The small size and geometry of the mass also ensures easier targeting; the size contributes to the surface area to volume ratio directly, and the geometry stipulates that diffusion occurs from the surrounding surface

to a shrinking core. This is in opposition to the capillary model, where diffusion from the capillary encounters an expanding radius, making targeting more difficult (*49*).

What can also be seen by comparing the micrometastasis model with vascularized tumors is that the parameter driving penetration is different. In answer to the question posed by Fujimori et al. (*27*), this model shows that diffusion is the dominant rate for targeting micrometastases, whereas transport across the vascular barrier, due to the low Biot number, is the dominant rate for vascularized tumors. Therefore, areas with hindered diffusion (*50*), such as collagen rich regions, are predicted to affect micrometastases more than vascularized tumors.

c. Vascularized Tumor Penetration Distances

Clearance Modulus Radius of Saturation. Setting $\Gamma_{tumor} = 1$ and solving for R, the maximum radius antibody will penetrate due to limitations from clearance is found to be:

$$R = \left(\sqrt{\frac{2PR_{cap}\left(A \cdot t_{1/2,\alpha} + B \cdot t_{1/2,\beta}\right)}{\ln(2) \cdot \left({[Ag]}/{\varepsilon} \right)}} \right) \cdot \sqrt{[Ab]_{plasma,0}} \qquad 15.$$

For bolus doses using typical parameter values (Tables 1 and 2):

$$R = factor \cdot 10^6 \, \mu m \left(\sqrt{\frac{(\mu g_{Ab})}{\left(\frac{\#Ag}{cell}\right)\left(\frac{cells}{mL}\right)}} \right) \qquad 16.$$

Mouse IgG in mouse factor = 65.6
Human IgG in mouse factor = 60.1
scFv in mouse factor = 33.3

Human IgG in human factor = 1.54
scFv in human factor = 1.02

The much larger plasma volume in humans (3 L in human vs. 2 mL in mouse) is responsible for the large difference in numerical factors. The antigen density is determined by the number of antigens per cell and cell density in tumors.

Thiele Modulus Radius of Saturation. Calculating the radius from the condition $\phi^2_{tumor} = 1$:

$$R = \left(\sqrt{\frac{D}{k_e \left({[Ag]_{tumor}}/{\varepsilon} \right)\left(1 + {1}/{Bi}\right)}} \right) \cdot \sqrt{[Ab]_{plasma}} \qquad 17.$$

Using typical parameter values (Figure 2 caption):

$$R_{scFv} = factor \cdot 10^6 \, \mu m \left(\sqrt{\frac{t_{1/2,endocytosis,hrs}\left(\mu g_{Ab}\right)}{\left(\frac{\#Ag}{cell}\right)\left(\frac{cells}{mL}\right)}} \right) \qquad 18.$$

scFv in human factor = 1.32
scFv in mouse factor = 41.6
IgG in human factor = 0.253
IgG in mouse factor = 8.01

The lesser of these two estimates of R (from $\phi_{tumor}^2 = 1$ or $\Gamma_{tumor} = 1$) will be the correct value, depending on which rate process is limiting (antibody consumption or plasma clearance, respectively).

The limitations presented above are sobering. For a modest antibody catabolism half-time of approximately one hour, over a milligram bolus dose of scFv or IgG is necessary in order to penetrate 100 μm away from tumor vasculature in a typical mouse xenograft. Since such doses are not likely to be practical in the clinical situation, increasing dosage cannot be solely relied upon to accomplish saturation. Rather, strategies to increase transport across the capillary wall must be developed to defeat the primary bottleneck in transport(*51, 52*).

d. Further Model Validation and Discussion

In the analysis by Adams et al.(*20*), even with an extended clearance time, a sharp front still develops with high affinity antibodies. This 'binding site barrier' effect cannot readily be explained by any mechanism related to clearance, given the high concentration, length of incubation, and lack of first pass clearance by the kidneys. The model predicts the presence of an apparent 'barrier' beyond which the antibody does not diffuse. This 'barrier,' however, reflects a dynamic competition between the relatively few antibodies (compared to the total amount of antigen present in the tumor) that diffuse across the capillary wall and into the tissue and the rate of internalization and catabolism of the antibody on the surface of the cells.

Trastuzumab provides a unique opportunity to study distribution in a second mouse xenograft model. Internalization and catabolism rates for the antibody have recently been measured directly(*44*), obviating the necessity to estimate internalization rates based on antigen turnover. This was utilized to examine the relationship between antibody dose and Thiele modulus from Baselga et al.(*53*); to saturate the entire tumor and fully suppress growth, doses giving a Thiele modulus approaching 1 are required. Incorporating the statistical distribution of measured distances from capillary to tumor cells(*22*), the attenuation of growth can be compared to the predicted targeted fraction of the tumor.

For the trastuzumab results presented in Figure 4, the cell killing effect is not extremely clear. In humans, the relative contribution of direct cytostatic effects (*54*), ADCC (*55*), and even tumor vasculature normalization (*56*) is not known. For the selected animal study with single agent administration, cytostatic effects and ADCC are responsible for suppressing tumor growth. $FcR\gamma^{-/-}$ nude mice show a lowered response to trastuzumab, but tumor growth is still reduced ~50% after 30 days, showing a contribution from cytostatic effects (*55*). ADCC assays with mouse splenocytes show weak cell killing activity using trastuzumab compared to human primary blood mononuclear cells (PBMCs), suggesting that ADCC is less prevalent in the animal model than in humans (*57*). Regardless of the mechanism of cell killing, significant targeting of the tumor is necessary for either effect(*58*).

Other experimental data can be used to validate the model, even if not all the parameters are known. (Parameters such as antigen density and internalization rates are necessary for complete validation so that no adjustable parameters are curve fit to the model.) The model predicts linear uptake with dose with either parameter being limited. This is found in several studies in addition to those mentioned in the paper(*59-64*). Previous models(*5*) have predicted that antibody uptake is proportional to the total concentration and amount of time spent in the blood before clearance (AUC). This has also been observed experimentally, and it is generally accepted that scFvs, although obtaining a better tumor to blood ratio due to their rapid clearance, also suffer from lower total uptake for the same reason(*65, 66*).

Some additional factors must be considered when interpreting total radioactive uptake in xenografts. Saturation may occur in certain regions prior to saturation of the entire tumor due to heterogeneous vascularization. This is one limitation of the model, since it is not able to analyze the bulk diffusion from a more heavily vascularized region to a sparsely vascularized region once saturation has started to occur. The residualizing nature of isotopes has been discussed previously.

e. Computational Validation of Scaling Parameters ϕ^2 and Γ

Full numerical simulations of equations 7-14 were performed to further test the validity of the simplifying assumptions used to derive the two saturation criteria. Antigen turnover was set to zero to test the clearance modulus alone, when $\phi^2 \rightarrow \infty$. Figure S1, A shows that for a clearance modulus less than 0.8 in all cases the full tumor volume for R = 100 μm is saturated with antibody. For micrometastases, saturation occurs over the range of 0.1-0.3 (Figure S1, B).

To examine the dependence of tumor saturation on the Thiele modulus, the value of steady antibody concentration was adjusted to vary the Thiele modulus, and different catabolism rates were considered as well. The simulations show that saturation occurs for $\phi_{\text{tumor}} < 0.7$ and $\phi_{\text{met}} < 0.4 - 1.0$ over a range of parameters. (Figure S1,C,D)

Several features present in the numerical simulations of Figure S1 can be conceptually explained based on the model. The tail at lower values of the clearance modulus for micrometastases is due to diffusion out of the micrometastasis once the plasma concentration drops significantly. The steeper curves present in the solid tumor simulations are a result of the capillary barrier. The high resistance of the capillary works in reverse and, without lymphatic drainage, the antibody is retained in the tumor longer, demonstrating one of the principles leading to the enhanced permeability and retention (EPR) effect (*67*). The clearance modulus indicates that for the long half lives of IgG molecules, extremely small amounts of antibody are needed in this limiting case. However, the amounts are so low that they are similar to the antibody K_d; a larger micrometastasis was simulated to avoid this unrealistic situation. Finally, Figure S1,D indicates that IgGs saturate the metastasis at a value larger than 1. For a zero-order reaction (catabolism at the rate of antigen turnover) in a sphere, the critical Thiele modulus for saturation occurs at a value of $\sqrt{6} \approx 2.45$. The slower diffusion of the IgG means it fulfills the shrinking core criteria better than the scFv (closer to a zero-order reaction), so the IgG curves are also steeper than the scFv curves.

Figure 4 is a contour plot of antigen saturation at the 95% level after a bolus dose. Antibody dose was adjusted to vary the clearance modulus using pharmacokinetic properties characteristic of antibodies and fragments. Both parameters depend on the concentration, so to independently vary the Thiele modulus, the catabolic rate constant was adjusted. In conditions where both parameters are near one, both mechanisms may contribute to poor penetration. For completely independent saturation criteria, a sharp corner would be expected in the plot at values of 1 for each modulus. The rounded corners in the plot indicate that the two parameters are not completely independent and saturation criteria are more strict when both parameters are close to 1. Conditions at the left and bottom sides of the figure approach the two limiting cases illustrated in Figure 1S.

In parameter space near the corner of the saturation curve, two major reasons exist for saturation not to occur. Antibody concentration, the driving force for penetration into the tumor, is just sufficient in either limiting case to saturate the tumor. For the clearance modulus, the initial assumption was that no antibody was consumed. Therefore, the antibody concentration needed for saturation is only sufficient for extravasation and diffusion to saturate the given volume. If antibody is consumed during this time, more antibodies will have to extravasate to bind the fresh antigen after catabolism has destroyed previously bound antibody. Similarly, the Thiele modulus provides the minimum concentration needed to overcome reaction in the tissue to reach the far 'edges' of tissue away from the capillary (or center of a micrometastasis). This assumes that the antibody concentration (driving force for diffusion) is constant. However, with a bolus dose, a finite time must pass to initially saturate tissue closer to the capillary before the antibody 'front' reaches tissue farther away. By the time this front of saturated antigen and free antibody reaches tissue farther away from the capillary, the antibody concentration driving force may not be high enough to overcome catabolism in the tissue. As the plasma antibody concentration drops, the number of antibodies extravasated decreases, and these may all be catabolized in the tumor tissue before it reaches more distant tissue. An analogous phenomenon happens with micrometastases. Other effects, such as the saturable kinetics of antibody catabolism affecting the diffusion concentration gradient, may have a smaller influence.

f. Applications to Imaging

The requirements for imaging using antibodies are different and not as strict as therapy. Every cell does not need to be targeted to achieve the desired result. However, analysis of the uptake of antibodies into this tissue is still important in achieving high specificity and a large signal. For some antigens, low doses of antibody are able to achieve a significant signal to background ratio, and agents such as CEA-scan often show a 'rim-sign' after administration due to convection and therefore better transport in the periphery of the tumor(*68*). Binding a larger fraction of the tumor is still desirable in many cases, however. For PET imaging, a larger signal may be able to increase the sensitivity to tumors less than 1 cm in diameter, roughly the current limit of detection. An increase in signal and specificity would also allow better detection using less expensive SPECT imaging devices as well. Compromises are evident when looking at the moduli, since a larger dose and longer clearance half life increase the tumor signal but also increase the time required for clearance and an acceptable background. The higher extravasation, diffusion, and rapid clearance of scFvs are desirable in this case due to the rapid targeting and decaying background. Pretargeting methods may be advantageous in this regard because they decouple the clearance of the antibody from the clearance of the imaging agent. This method also alleviates the need to match the radioisotope half life with the antibody clearance rate. A slow clearing antibody can achieve significant targeting, clear from the circulation, and bind a rapidly decaying, rapidly cleared isotope given at a later time just prior to imaging.

g. Applications to Radioimmunotherapy

This model primarily addresses the obstacles of getting antibodies to the site of tumor tissue. However, in addition to targeting all tumor cells, other considerations must go into the design of RIT therapy, such as the choice of radioisotope in the treatment protocol. Ideally, antibodies would reach and saturate every tumor cell, and the decay from each isotope would contribute directly to cell killing. An isotope with a short range and highly lethal decay would be able to target each cell specifically with little dose outside of the tumor or metastasis. The half-life for decay would be slow compared to clearance to limit decay in the normal tissue but rapid compared to retention in the tumor so a large amount of energy is deposited in the cancerous tissue. However, these ideal conditions are not possible in all cases and represent the main limitations of RIT.

When targeting micrometastases with RIT, an ideal range for the radiation would be several cell diameters (10 to a couple 100 μm). Since these metastases are only a few hundred μm in diameter, a longer range only contributes to toxicity of normal tissue. A range of a few cell diameters obviates the need for internalization and allows for some 'cross-fire' to target low-antigen or antigen-negative cells adjacent to targeted cells. Alpha emitters possess ranges on this scale, and they are likely some of the best candidates for this type of therapy. The high LET of the alpha particles also makes these isotopes particularly attractive for tumor therapy. They have a high probability of cell kill after only a few traversals and a low sensitivity to variations in cell cycle and oxygenation. The question of secondary toxicity still needs to be more adequately addressed, but these radioisotopes look promising(*69*).

Low energy electron emitters have a very short range and possess some properties similar to high LET radiation. Their range can become limiting, however, since it may not be able to reach the nucleus from the surface of the cell. In this instance, the antigen must be internalized in order to reach the nucleus, and these isotopes are then under similar restrictions as immunotoxins. The rate of internalization must be significant enough to get a toxic amount of product into the cell but slow enough that the antibody can penetrate deep into the tissue (i.e. maintain a Thiele modulus less than 1).

Beta emitters are commonly used in RIT studies. Their range is one property that sets this class of isotopes apart from the others. The ranges can be several millimeters in tissue, both to their advantage and detriment. In large, heterogeneous tumors with significant necrotic regions far from blood vessels, the effective radius (R) for some areas is so large that it is not practical to achieve a Thiele and/or clearance

modulus less than 1. The long range of beta particles can deposit their energy at these larger distances to induce cell killing in these regions. The large range unfortunately also delivers a large amount of energy to surrounding healthy tissue. The low LET from the beta radiation is not as advantageous as high LET energy, but the potential for cell repair in normal tissue may make these less toxic to secondary tissues. Using more than one radioisotope for treating micrometastases versus solid tumors may allow the benefits of the short range of alpha particles to be paired with the longer range of beta emitters for more comprehensive therapy.

h. Targeting Improvement

Systematic consideration of each of the parameters in Equations 1-6 provides suggestions for directions to improve tumor saturation with antibody therapeutics, bearing in mind that smaller values of ϕ^2 and Γ are desirable, while larger values of the Biot number are sought. Additional items that those mentioned previously are discussed below.

Antibody Dose ($[Ab]_{plasma,0}$)

Capillary wall resistance, exemplified by the small Biot number, necessitates very high plasma levels for sufficient targeting in tumors. Dose represents a real limit to radioisotopes directly conjugated to antibodies and fragments due to secondary toxicity. Higher antibody concentrations increase the dose to bone marrow and other normal tissues, and uptake of fragments by the kidney can cause limiting renal toxicity. The addition of cold antibody allows penetration deeper into the tissue without increasing secondary toxicity, but pretargeting techniques may also be necessary to obtain better signal (for imaging) or cell killing (for therapy). Current clinical values are in the single-digit micromolar concentration range for naked antibody therapeutics. For therapeutics currently on the market, such as trastuzumab, continuous high dosing (~0.9 μM(*70*)) and antibody recycling may contribute to their success. Even higher doses are used (3 times larger) for more convenient delivery(*70*).

Systemic Clearance ($A, t_{1/2,\alpha}, B, t_{1/2,\beta}$)

Minimizing Γ is most straightforwardly accomplished by increasing circulation time in the blood - for antibody fragments, this has been accomplished by pegylation or attachment (covalently or noncovalently) to albumin. Fc engineering can also decrease systemic clearance(*71*). Correspondingly increasing exposure to healthy tissue, such as bone marrow, may limit this approach for antibodies carrying cytotoxic payload conjugates (e.g. radioisotopes, chemotherapeutics, toxins).

Diffusivity (D)

It has been found that diffusivity of macromolecules in tissues and gels is approximately inversely proportional to molecular weight, supporting the use of smaller fragments for greater penetration. It should be noted however, that lowering the molecular weight below the renal filtration limit (~60 kDa) can lead to catastrophic increases in Γ. Fast clearance rates do allow for better imaging; the plasma levels decay rapidly while antibody load in the tumor is still high, so antibody fragments achieve a high tumor/plasma ratio. For imaging, not every cell has to be targeted, only a large enough number to obtain a significant signal to noise ratio. However, for tumor saturation, a goal of most therapies, rapid systemic clearance is a definite drawback since the plasma concentration drops too rapidly for saturation to occur. As in most such cases of counteracting trends (i.e. costs of rapid clearance vs. benefits of rapid diffusion), one expects an optimal value for this parameter to exist that best balances these tendencies, likely near the renal filtration limit in size.

Net Endocytic Consumption Rate (k_e)

A consideration extensively explored here is that of antigen turnover and antibody metabolism. Our analysis indicates that antigen or receptor turnover, even at rates equal to or lower than lipid membrane turnover, severely limits penetration into the tissue. Thus administering high doses over long periods of time does not guarantee targeting of all tumor antigens. Depth of tissue penetration is determined by a competition between rates of extravasation and turnover within the tumor. The turnover rates for several

antibodies and clinically approved drugs are high enough to affect targeting in these tissues(*6, 7, 44*). k_e should be minimized in most cases. This strategy is appropriate for exploiting Fc effector functions for tumor cell-killing, and for multi-step strategies such as pretargeted radioimmunotherapy or antibody-directed enzyme prodrug therapy.

Antigen Expression Level ([Ag])

Tumor-associated antigen targets are generally chosen due to high levels of expression, in addition to lesser expression on normal tissue. For potent payloads, addition of excess unconjugated competitor antibody could effectively lower available antigen binding site concentration [Ag] and thereby allow better tumor penetration, without correspondingly lowering the payload delivery sufficiently far to sacrifice significant tumor-killing potential. It is tempting to speculate that such an effect may be at play in the current dosing strategies for anti-CD20 radioimmunotherapy, which include a cold bolus dose of antibody before administration of the radioconjugated drug. Surface antigen dosage can also be reduced by large-scale crosslinking of antibodies for some GPI-tailed antigens and transmembrane proteins(*34, 72*). By contrast to highly potent payloads such as alpha-emitting radioisotopes, ADCC depends on a high surface density of Fc domains to trigger effector functions via the Fc receptors of macrophages and natural killer cells(*73*). Effective antagonism of growth promoting signals by ErbB receptors also requires nearly complete blockage of receptors(*74*). Consideration of the {minimum required potency}-vs.-{acceptable penetration} tradeoff might also lead to selection of tumor antigens with more modest levels of tumor expression with negligible healthy tissue expression.

Rate of Capillary Exit (*P*)

The particular difficulties in penetrating vascularized tumors are highlighted by the very small value of the Biot number; enhancement of the vascular permeability coefficient *P* must be sought to overcome this limitation. By comparison to avascular spheroidal cell clumps in well perfused normal tissue, the rate of antibody extravasation from capillaries severely limits antibody delivery. For previously reported parameter values, the Biot number is much less than one. Poor vascularization means fewer vessels are responsible for delivering antibodies to the entire tumor mass. The intrinsic macroscopic heterogeneities in blood supply and antigen expression require even higher levels of targeting so antibodies can diffuse from more easily saturated areas to those areas less accessible and with more stringent conditions (e.g. higher antigen load).

Tumor Geometry Factors (R, ε, R_{cap})

The effect of extracellular matrix composition (collagen vs. hyaluronan) on accessible volume fraction and diffusivity has been examined, as well as strategies for altering it(*75*). Although transient vascular normalization from anti-angiogenic factors may alter R_{cap}, one would not expect significant changes in Γ to result.

Figure S1 Full numerical simulations were performed with the endocytosis rate constant set to 0 (panels A,B) or constant plasma concentrations (panels C,D). The endocytosis rate for the bottom panels was varied from $4x10^{-6}$ s^{-1} (~48 hr half life) to $4x10^{-5}$ s^{-1} (~5 hr half life) to $4x10^{-4}$ s^{-1} (~30 minute half life). Using the pharmacokinetic parameters in Table 1, antibody concentrations were varied to determine saturation of tissue 100 μm from the capillary wall or at the center of a 100 μm radius metastasis (300 μm radius for IgGs in panel d). Antigen concentration = 0.3 μM , capillary radius = 10 μm, k_{on} = $1x10^{5}$ $M^{-1}s^{-1}$, permeability = $3x10^{-9}$ m/s for IgG and $5x10^{-9}$ m/s for scFv, Kd = 1 nM for IgG and 0.1 nM for scFv, ε = 0.1 for IgG and 0.3 for scFv, D = $14x10^{-12}$ m^2/s for IgG and $80x10^{-12}$ m^2/s for scFv. The normal tissue parameters were: lambda = $8.9x10^{-5}$, kappa = $4.6x10^{-5}$ for IgG and $1x10^{-4}$ for scFv. Extra simulations were also run for 3 hour infusions in the top left panel.

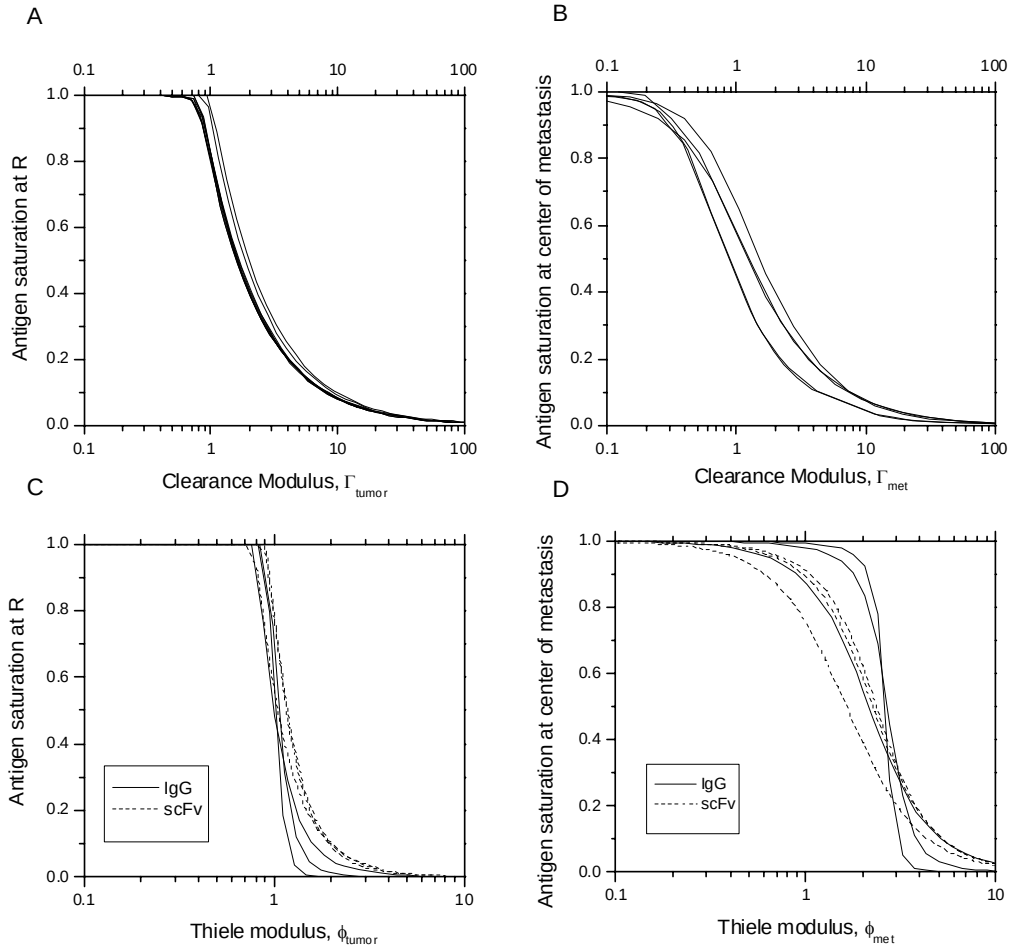

B. References for Model Parameters Used in Simulations

Table 1 - Model Values Used for Simulations

Parameter	Adams et al.	Baselga et al.	References
Model	Nephrectomized Mouse Xenograft	Multiple Dose Mouse Xenograft	
R	'300 μm'	100 μm	(*22*)
K_d	15 pM	5 nM	(*20*), (*53*)
R_{cap}	5 μm	10 μm	(*76*, *77*)
D	80 $\mu m^2/s$	14 $\mu m^2/s$	(*5*)
P	$5x10^{-9}$ m/s	$3x10^{-9}$ m/s	(*77*)
Ag	0.15 μM	0.13	(*42*, *53*, *78*)
epsilon	0.3	0.1	(*79*)
Ab	2 μM	varies	2 mL plasma volume or 78 mL/kg for mice; 3 L for human
$k_{endocytosis}$	$2.2x10^{-4}$ /s	$2.2x10^{-4}$ x 0.15 = $3.3x10^{-5}$ /s	(*35*, *44*, *80*)

Estimates for cell density in vascularized tumors range from $1x10^8$ to $1x10^9$ cells/mL (typically 2-$4x10^8$ cells/mL) and can be approximated from histological images (*42*, *49*, *78*). Expression levels may vary *in vitro* versus *in vivo*, however, and a low void fraction may lower the accessible antigen. The effective void fraction, ε, is estimated at 0.1 for IgGs and 0.3 for scFvs (*79*). For example, *in vivo* CEA levels were determined to be approximately one half of that found *in vitro* (*81*) and are highly variable.

The binding rate for the scFv in Adams et al. was obtain from a previous study(*82*).

Table 2 - Characteristic Pharmacokinetic Parameters

Whole Body Pharmacokinetic Parameters	alpha	beta	% α	Ref.
Mouse IgG in Mouse	1 day	7 days	70%	(*83*)
Human IgG in Mouse	1.2 hr	6.81 days	66%	(*84*)
Human IgG in Human	12.74 hrs	86.92 hrs	43%	(*85*)
scFv in mouse	0.05 hr	3 hrs	80%	(*86*)
scFv in human	0.42 hrs	5.32 hrs	90%	(*65*)

C. Derivation of Clearance Modulus for Solid Tumors

This derivation applies to the shrinking core model in an 'inside-out' cylindrical geometry. It is a limiting case where no catabolism of the antibody occurs in the tissue, only binding. It is assumed that the binding reaction occurs much faster than diffusion and the antigen is in excess over the free antibody, causing a slow moving reaction front. The binding reaction is much faster than diffusion, which is faster than the rate of movement of the front; thus a pseudo-steady state develops with an instantaneous reaction at the surface of the complex/free-antigen boundary. The analysis is carried out for high affinity antibodies where the dissociation rate is slow enough to assume irreversible binding. In this model, a mixed or Robin boundary condition is used to incorporate the large resistance across the capillary wall at the center of the cylinder. In part B, it is also assumed the antibody gradient develops and changes rapidly in comparison with the plasma decay, providing a pseudo-steady state with decaying plasma concentrations.

Part A – Derivation for saturation time for solid tumor with constant plasma concentration:

Assuming a pseudo-steady state develops:

$$\frac{D}{r}\frac{d}{dr}r\frac{d[Ab]}{dr}=0$$
$$\int\frac{d}{dr}r\frac{d[Ab]}{dr}=\int 0$$
$$[Ab]=K_1\ln(r)+K_2$$

For the boundary conditions:

B.C. 1: Instantaneous reaction

$[Ab]$ = 0 at r = R(t)

B.C. 2: Mixed boundary condition at the capillary wall (r = $R_{capillary}$)

Flux across capillary wall = Flux just outside capillary wall

$$P\cdot\left(\left(\varepsilon\cdot[Ab]_{plasma}\right)-[Ab]\right)=-D\left(\frac{d[Ab]}{dr}\right)$$

so:

$$\varepsilon\cdot[Ab]_{plasma}=-\frac{D}{P}\left(\frac{d[Ab]}{dr}\right)+[Ab]\qquad\text{at r = }R_{capillary}$$

This second boundary condition follows those of a mixed or Robin boundary condition where both the value and derivative are involved.

Using BC 1:

$$[Ab]=K_1\ln\left(\frac{r}{R}\right)$$

Using BC 2:

$$K_1=\frac{\varepsilon\cdot[Ab]_{plasma}}{\left(\frac{-D}{P\cdot R_{cap}}+\ln\left(\frac{R_{cap}}{R}\right)\right)}$$

The concentration profile is then:

$$[Ab]=\frac{\varepsilon\cdot[Ab]_{plasma}}{\left(\frac{D}{P\cdot R_{cap}}+\ln\left(\frac{R}{R_{cap}}\right)\right)}\ln\left(\frac{R}{r}\right)$$

To determine the rate of 'erosion' of the cylinder, a differential volume at the radius of saturation is defined. Assuming instantaneous reaction/binding, the number of molecules entering the volume (product

of flux and area) in a differential time is equal to the number of molecules reacting/binding in that volume. Since this occurs instantaneously, the number of reacting molecules is equal to the total number of binding sites within the volume (the initial antigen concentration).

Using overall concentration for both sides of the equation:

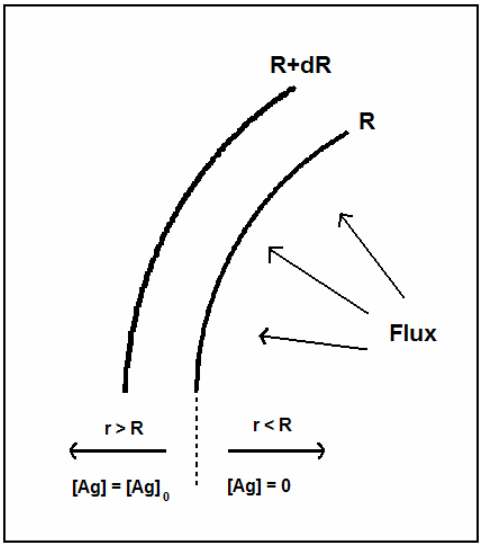

# of binding sites = # of binding antibodies

$$[Ag]_0 (2\pi RL) dR = flux\big|_{r=R} (2\pi RL) dt$$

$$[Ag]_0 \frac{dR}{dt} = -D \frac{d[Ab]}{dr}\bigg|_{r=R}$$

Taking the derivative of the concentration profile (above):

$$[Ag]_0 \frac{dR}{dt} = -D \frac{-\varepsilon \cdot [Ab]_{plasma}}{\left(\frac{D}{P \cdot R_{cap}} + \ln\left(\frac{R}{R_{cap}} \right) \right)} \frac{1}{r}\bigg|_{r=R}$$

$$R \frac{dR}{dt} = \frac{\varepsilon D [Ab]_{plasma}}{[Ag]_0 \left(\frac{D}{P \cdot R_{cap}} + \ln\left(\frac{R}{R_{cap}} \right) \right)}$$

For low Biot number, the second term (containing $\ln(R/R_{cap})$) is negligible, and the integration can be carried out neglecting this term. (e.g. for R/R_{cap}=30 and estimates for the Biot number (*77, 81*), 467 >> 3.4 for IgG and 1600 >> 3.4 for scFv). However, for completeness, we will include this term for now.

$$\left(\frac{D}{P \cdot R_{cap}} + \ln\left(\frac{R}{R_{cap}} \right) \right) R \cdot dR = \frac{\varepsilon D [Ab]_{plasma}}{[Ag]_0} dt$$

with a dummy variable (x) for R:

$$\frac{D}{P \cdot R_{cap}} \int_{R_{cap}}^{R} x \cdot dx + \int_{R_{cap}}^{R} \ln\left(\frac{x}{R_{cap}} \right) x \cdot dx = \frac{\varepsilon D [Ab]_{plasma}}{[Ag]_0} \int_0^{t_{sat}} dt$$

$$\left(\frac{D}{P \cdot R_{cap}} - \ln(R_{cap}) \right) \left(\frac{R^2}{2} - \frac{{R_{cap}}^2}{2} \right) + \frac{R^2}{2} \ln(R) - \frac{R^2}{4} - \frac{{R_{cap}}^2}{2} \ln(R_{cap}) + \frac{{R_{cap}}^2}{4} = \frac{D \cdot [Ab]_{plasma}}{[Ag]_0 / \varepsilon} t_{sat}$$

Making assumptions to simplify:

1. If $R >> R_{cap}$, will integrate from 0 to R instead of R_{cap} to R.

$$\left(\frac{D}{P\cdot R_{cap}}-\ln(R_{cap})\right)\left(\frac{R^2}{2}\right)+\frac{R^2}{2}\ln(R)-\frac{R^2}{4}=\frac{D\cdot[Ab]_{plasma}}{[Ag]_0/\varepsilon}t_{sat}$$

$$\left(\frac{D}{P\cdot R_{cap}}+\ln(\frac{R}{R_{cap}})-\frac{1}{2}\right)=\frac{2D\cdot[Ab]_{plasma}}{R^2[Ag]_0/\varepsilon}t_{sat}$$

2. If $\frac{D}{P\cdot R_{cap}} >> \ln\left(\frac{R}{R_{cap}}\right)$ and >> 1/2 as shown above, then it simplifies to one term:

$$t_{sat}=\frac{\left([Ag]_0/\varepsilon\right)R^2}{\left(2\cdot[Ab]_{plasma}\cdot P\cdot R_{cap}\right)}$$

Part B – Using saturation time and AUC for decaying plasma concentration to define Clearance modulus

For decaying boundary conditions, a few assumptions are necessary for the simplified derivation. If the plasma concentration is dropping, it will be assumed that the changes in the concentration profile will respond rapidly such that a pseudo-steady state exists with decaying boundary conditions.

With the shrinking core model, there is no reaction outside the core, so the pertinent time scale is R^2/D. The time scale for plasma decay is the half life.

Assuming:

$$t_{clearance\_half\_life} > \frac{R^2}{D}$$

For a small antibody fragment with D = 80 μm²/s and R = 300 μm, the half life must be greater than 20 minutes. For large fragment with D = 14 μm²/s, the half life must be greater than 1 hour and 45 minutes. For a scFv and IgG respectively, these assumptions are generally true. It is also not as strict as it initially appears, since the relevant R value is initially small before much of the tumor is saturated. This corresponds with the most rapid drop in plasma concentration. Therefore, when the boundary conditions are changing the most rapidly, the system responds much faster than at later time points.

The boundary conditions for infusion and decay vary over time:

$$[Ab]_{plasma}=[Ab]_{plasma,0} \qquad 0<t<t_{\inf usion}$$
$$[Ab]_{plasma}=[Ab]_{plasma,0}\left(A\exp(-k_\alpha t)+B\exp(-k_\beta t)\right) \qquad t_{\inf usion}<t<\infty$$

where A and B are the fractions of alpha and beta clearance.

In part A, the equation was integrated before making simplifying assumptions. Here it will be simplified before integration.

From part A:

$$R\frac{dR}{dt} = \frac{\varepsilon D[Ab]_{plasma}}{[Ag]_0\left(\frac{D}{P \cdot R_{cap}} + \ln\left(\frac{R}{R_{cap}}\right)\right)}$$

Using an estimate for the second term in the denominator:

$$\ln\left(\frac{R}{R_{cap}}\right) = 3.4$$

when R_{cap} = 10 μm and R = 300 μm.

Assuming:

$$\frac{D}{P \cdot R_{cap}} >> 3.4$$

For a typical values, R_{cap} = 10 μm, D = 80 $\mu m^2/s$, and P = $5x10^{-3}$ μm/s:

$$\frac{D}{P \cdot R_{cap}} = 1600 >> 3.4$$

Then:

$$R\frac{dR}{dt} = \frac{\varepsilon D[Ab]_{plasma}(t)}{[Ag]_0\left(\frac{D}{P \cdot R_{cap}}\right)} = \frac{[Ab]_{plasma}(t) \cdot P \cdot R_{cap}}{[Ag]_0 / \varepsilon}$$

where the (t) indicates that $[Ab]_{plasma}$ is a function of time.

This provides the much simpler integration as discussed in part A. Using the simplified equation from above and integrating over the infusion period:

$$\int_{R_{cap}}^{R_{temp}} RdR = \int_0^{t_{infusion}} \frac{[Ab]_{plasma}(t) \cdot P \cdot R_{cap}}{[Ag]_0 / \varepsilon} dt$$

Where R_{temp} is the radius of saturation after the infusion period before decay.

Ignoring the R_{cap} term on the LHS (as in part A R_{cap} << R):

$$\frac{R_{temp}^{\ 2}}{2} = \frac{[Ab]_{plasma} \cdot P \cdot R_{cap}}{[Ag]_0 / \varepsilon} t_{infusion}$$

The second period occurs when the antibody decays from the plasma. To obtain the maximum radius that could be saturated assuming no catabolism and irreversible binding, the RHS is integrated to infinity. The LHS is then integrated to R_{max}, the maximum achievable radius of saturation.

Integrating over the second time period:

$$\int_{R_{temp}}^{R_{\max}} R dR = \int_{t_{\inf usion}}^{\infty} \frac{[Ab]_{plasma}(t) \cdot P \cdot R_{cap}}{[Ag]_0 / \varepsilon} dt$$

$$\int_{R_{temp}}^{R_{\max}} R dR = \frac{[Ab]_{plasma,0} \cdot P \cdot R_{cap}}{[Ag]_0 / \varepsilon} \int_{t_{\inf usion}}^{\infty} \left(A \exp(-k_\alpha t) + B \exp(-k_\beta t) \right) dt$$

$$\frac{R_{\max}^{\ 2}}{2} - \frac{R_{temp}^{\ 2}}{2} = \frac{[Ab]_{plasma,0} \cdot P \cdot R_{cap}}{[Ag]_0 / \varepsilon} \left(\frac{A}{k_\alpha} \exp(-k_\alpha t_{\inf usion}) + \frac{B}{k_\beta} \exp(-k_\beta t_{\inf usion}) \right)$$

Adding equations together:

$$\frac{R_{\max}^{\ 2}}{2} = \frac{[Ab]_{plasma,0} \cdot P \cdot R_{cap}}{[Ag]_0 / \varepsilon} \left(t_{\inf usion} + \frac{A}{k_\alpha} \exp(-k_\alpha t_{\inf usion}) + \frac{B}{k_\beta} \exp(-k_\beta t_{\inf usion}) \right)$$

Solving for t_{sat} on the LHS (see part A):

$$\overbrace{\left(\frac{R_{\max}^{\ 2} \left([Ag]_0 / \varepsilon \right)}{2 \cdot [Ab]_{plasma,0} \cdot P \cdot R_{cap}} \right)}^{t_{sat}} = \overbrace{\left(t_{\inf usion} + \frac{A}{k_\alpha} \exp(-k_\alpha t_{\inf usion}) + \frac{B}{k_\beta} \exp(-k_\beta t_{\inf usion}) \right)}^{normalized\_AUC}$$

This equation illustrates that the saturation time for the maximum volume of tissue (LHS) is equal to the normalized AUC (RHS). The Area Under the Curve (AUC) is the integral of the plasma concentration over time:

$$AUC = \int [Ab]_{plasma}(t) dt$$

and the normalized AUC is:

$$\text{normalized } AUC \equiv \frac{\int [Ab]_{plasma}(t) dt}{[Ab]_{plasma,0}}$$

Taking the ratio of saturation time (LHS) to normalized AUC (RHS):

$$1 = \frac{R_{\max}^{\ 2} \left([Ag]_0 / \varepsilon \right)}{2 \cdot [Ab]_{plasma,0} \cdot P \cdot R_{cap} \left(t_{\inf usion} + \frac{A}{k_\alpha} \exp(-k_\alpha t_{\inf usion}) + \frac{B}{k_\beta} \exp(-k_\beta t_{\inf usion}) \right)}$$

The clearance modulus is then defined as:

$$\Gamma \equiv \frac{R^2\left([Ag]_0 \big/ \varepsilon\right)}{2 \cdot [Ab]_{plasma,0} \cdot P \cdot R_{cap}\left(t_{\inf usion} + \frac{A}{k_\alpha}\exp(-k_\alpha t_{\inf usion}) + \frac{B}{k_\beta}\exp(-k_\beta t_{\inf usion})\right)}$$

Comparing the ratio to the defined clearance modulus, it is apparent that if R is larger than the R_{max} given the other conditions, the clearance modulus will be greater than 1 and the tissue of radius R will not be saturated. If $R < R_{max}$ (i.e. the cylinder of tissue is smaller than the maximum cylinder of tissue that could be saturated), then the clearance modulus will be less than one. Notice that over an infinite period, the assumptions about no catabolism and irreversible binding will break down. This is one reason why the clearance modulus must be less than and not equal to one.

If a constant plasma concentration is maintained over an indefinite period of time, the clearance modulus approaches 0. Given a long enough period of time, any size cylinder with an arbitrary plasma concentration should saturate. *However*, this is assuming absolutely no catabolism in the tissue.

Alternatively, the clearance modulus can be defined using half-lives instead of clearance rate constants:

$$\Gamma \equiv \frac{R^2\left([Ag]_0 \big/ \varepsilon\right)}{2 \cdot [Ab]_{plasma,0} \cdot P \cdot R_{cap}\left(t_{\inf usion} + \frac{At_{1/2,\alpha}}{\ln(2)}\exp(-\frac{t_{1/2,\alpha}}{\ln(2)}t_{\inf usion}) + \frac{Bt_{1/2,\beta}}{\ln(2)}\exp(-\frac{t_{1/2,\beta}}{\ln(2)}t_{\inf usion})\right)}$$

Simplifying for various cases:

Case 1: Bolus dose only, no infusion

$$\Gamma \equiv \frac{\ln(2) \cdot R^2 [Ag]_0 \big/ \varepsilon}{2 \cdot [Ab]_{plasma,0} \cdot P \cdot R_{cap}\left(A \cdot t_{1/2,\alpha} + B \cdot t_{1/2,\beta}\right)}$$

Case 2: Single exponential

$$\Gamma \equiv \frac{R^2 [Ag]_0 \big/ \varepsilon}{2 \cdot [Ab]_{plasma,0} \cdot P \cdot R_{cap}\left(t_{\inf usion} + \frac{t_{1/2,clearance}}{\ln(2)}\exp(-k_{clearance}t_{\inf usion})\right)}$$

Case 3: No infusion AND single exponential

$$\Gamma \equiv \frac{\ln(2) R^2 [Ag]_0 \big/ \varepsilon}{2 \cdot [Ab]_{plasma,0} \cdot P \cdot R_{cap} \cdot t_{1/2,clearance}}$$

D. Derivation of Thiele Modulus for Micrometastases and Solid Tumors (No Capillary Resistance)

The Thiele modulus is derived for the second limiting case being examined in this paper. For this derivation, the plasma concentration is held constant until a steady state develops in the sphere or cylinder of tissue. The analysis is carried out when the reaction front has reached its maximum (steady state) radius. Thus, the antibody extravasating from the capillary or diffusing into the spheroid is all catabolized within the tissue.

Note, Ab and Ag are defined in terms of overall tumor volume.

Free Antibody Balance

$$\frac{\partial Ab}{\partial t} = D_{eff}\,\frac{1}{r}\frac{\partial}{\partial r}\left(r\frac{\partial Ab}{\partial r}\right) - \frac{k_{on}}{\varepsilon}AbAg + k_{off}B^{*} \qquad \text{ia.} \quad \text{(cylindrical)}$$

$$\frac{\partial Ab}{\partial t} = D_{eff}\,\frac{1}{r^{2}}\frac{\partial}{\partial r}\left(r^{2}\frac{\partial Ab}{\partial r}\right) - \frac{k_{on}}{\varepsilon}AbAg + k_{off}B^{*} \qquad \text{ib.} \quad \text{(spherical)}$$

Bound Antibody-Antigen Complex Balance

$$\frac{\partial B^{*}}{\partial t} = \frac{k_{on}}{\varepsilon}AbAg - k_{off}B^{*} - k_{e}B^{*} \qquad \text{ii.}$$

Free Antigen Balance

$$\frac{\partial Ag}{\partial t} = R_{s} - \frac{k_{on}}{\varepsilon}AbAg + k_{off}B^{*} - k_{e}Ag \qquad \text{iii.}$$

where Ab is the antibody concentration, Ag is the antigen concentration, and B^{*} is the bound antibody-antigen complex. k_{on}, k_{off}, k_e, D_{eff}, and R_s are the binding rate, dissociation rate, endocytosis/catabolism rate, diffusion coefficient, and antigen synthesis rate constants, respectively. The square brackets representing concentration have been dropped for ease of notation in this derivation.

Invoke Steady State Assumption

As previously noted, the Thiele modulus is derived when the system has reached steady state. Thus, the antibody, bound complex, and free antigen concentrations are not changing over time. The reaction front is stationary due to the fact that the antibody extravasating from the capillary or diffusing into the metastasis is degraded before reaching the reaction front.

Defining dimensionless values for radius, antibody, antigen, and bound complex:

$$\rho \equiv \frac{r}{R} \qquad A \equiv \frac{Ab}{Ab_{0}} \qquad G \equiv \frac{Ag}{Ag_{0}} \qquad B \equiv \frac{B^{*}}{Ag_{0}}$$

where R is the arbitrary radius of interest, Ab_0 is the antibody concentration at the surface of a micrometastasis or just outside the capillary in the tissue (per overall tumor volume), and Ag_0 is the initial antigen concentration in the tissue (per overall tumor volume).

Note: For Section B of Supplemental, A and B are used as defined above (not as defined in the list of symbols).

Non-dimensionalize and simplify i.

$$0 = \nabla^2 A - \frac{k_{on} R^2 Ag_0}{\varepsilon \cdot D_{eff}} AG + \frac{k_{off} R^2 Ag_0}{DAb_0} B \qquad \text{i'.}$$

Non-dimensionalize and simplify ii.

$$B = \left(\frac{k_{on}}{k_{off} + k_e} \right) \frac{Ab_0}{\varepsilon} AG \qquad K_d \equiv \frac{k_e + k_{off}}{k_{on}}$$

$$B = \left(\frac{Ab_0}{\varepsilon \cdot K_d} \right) AG \qquad \text{ii'.}$$

Non-dimensionalize and simplify iii.

$$0 = k_e Ag_0 R - \frac{k_{on}}{\varepsilon} Ab_0 Ag_0 AG + k_{off} Ag_0 B - k_e Ag_0 G \qquad R = \frac{R_s}{k_e Ag_0}$$

$$0 = k_e R - \frac{k_{on}}{\varepsilon} Ab_0 AG + k_{off} B - k_e G \qquad \text{iii'.}$$

Plug ii' into i'

$$0 = \nabla^2 A - \frac{k_{on} R^2 Ag_0}{\varepsilon \cdot D_{eff}} AG + \frac{k_{off} R^2 Ag_0}{DAb_0} \left(\frac{Ab_0}{\varepsilon \cdot K_d} AG \right)$$

$$0 = \nabla^2 A - \left[\left(\frac{R^2 Ag_0}{\varepsilon \cdot D_{eff}} AG \right) \left(\frac{k_e}{K_d} \right) \right] \qquad \text{ii'+i'}$$

Plug ii' into iii'

$$0 = k_e R - \frac{k_{on}}{\varepsilon} Ab_0 AG + k_{off} \left(\frac{Ab_0}{\varepsilon \cdot K_d} \right) AG - k_e G$$

$$G \left(\frac{Ab_0 A}{\varepsilon \cdot K_d} + 1 \right) = R \qquad \text{Assuming surface conc. is constant for steady state, R=1}$$

$$\text{ii'+iii'}$$

$$G = \frac{1}{\left(\frac{Ab_0 A}{\varepsilon \cdot K_d} + 1 \right)}$$

Combine ii'+iii' and ii'+i'

$$0 = \nabla^2 A - \left(\frac{R^2 Ag_0 k_e}{\varepsilon \cdot D_{eff} K_d} \frac{A}{\left(\frac{Ab_0 A}{\varepsilon \cdot K_d} + 1 \right)} \right)$$

$$0 = \nabla^2 A - \left(\frac{R^2 Ag_0 k_e}{D_{eff} Ab_0} \frac{A}{\left(A + \frac{\varepsilon \cdot Kd}{Ab_0} \right)} \right)$$

$$0 = \nabla^2 A - \Phi^2 \left[\frac{A}{\left(A + Kd \cdot \varepsilon / Ab_0 \right)} \right]$$

Define $\phi^2 = \left(\frac{R^2 Ag_0 k_e}{DAb_0} \right)$

$$\boxed{\phi^2 = \left(\frac{R^2 \left([Ag]_0 / \varepsilon \right) k_e}{D[Ab]_{\text{int}}} \right)}$$

where $[Ab]_{\text{int}} = \frac{Ab_0}{\varepsilon}$

$[Ab]_{int}$ is the interstitial antibody concentration at the surface of the tissue. For micrometastases, $[Ab]_{int}$ is the concentration at the surface of the spheroid. For a constant infusion:

$$[Ab]_{\text{int}} = \frac{\kappa}{\lambda} \cdot [Ab]_{plasma}$$

$[Ab]_{int}$ is affected by the capillary resistance for solid tumors, and thus the analysis is more complicated. The next section shows a simplified way of finding $[Ab]_{int}$ from the plasma concentration for solid tumors.

E. Derivation of Thiele Modulus with Capillary Resistance

To obtain a simple scaling argument for saturation from the above Thiele modulus equation with Robin boundary conditions and cylindrical geometry, a few more assumptions must be made. The main difficulty arises in that the plasma concentration is known, but the concentration just outside the capillary wall (Ab_0 from the previous section) is unknown. To define the Thiele modulus in terms of known parameters (i.e. $[Ab]_{plasma}$ instead of $[Ab]_{int}$), the boundary conditions and a mass balance will have to be utilized. An assumption will also be made about the value of the Thiele modulus to further generalize the result.

As in the clearance modulus, the shrinking core assumptions will be invoked such that a (stalled) reaction front exists with the antigen being completely saturated prior to this front ($[Ag] = 0$, $[B] = [Ag]_0$).

Mass Balance and no flux boundary condition

At steady state after the reaction front has reached its maximum value, the flux of antibody across the capillary wall will be equal to the consumption within the radius of saturated tissue. Because the antibody is assumed not to diffuse beyond this reaction front, the no-flux boundary is not necessary to define the volume of interest. However, it does reinforce the idea that no antibody leaves the system other than what is catabolized.

At steady state:

Flux across the capillary wall = Catabolism in the tissue

$$flux\big|_{r=R_{cap}} S = k_e [B] V = k_e [Ag]_0 V$$

$$flux\big|_{r=R_{cap}} = \frac{k_e [Ag]_0}{S/V}$$

where k_e is the catabolic turnover of antigen, $[Ag]_0$ is the concentration of antigen over the tumor volume, S is the surface area of capillary, and V is the volume of saturated tumor. This is defined with respect to the overall antigen concentration.

Robin boundary condition at capillary wall

$$flux\big|_{r=R_{cap}} = P\cdot\left([Ab]\big|_{r=R_{cap}-} - [Ab]\big|_{r=R_{cap}+}\right) = P\cdot\left(\left(\varepsilon\cdot[Ab]_{plasma}\right) - [Ab]_{cap}\right)$$

where P is the vascular permeability, $[Ab]_{plasma}$ is the plasma concentration of antibody, and $[Ab]_{cap}$ (same as Ab_0 from the previous section) is the *overall* concentration of antibody on the abluminal side of the capillary (*9*). Note that ε is required so both concentrations are on an overall tumor volume basis.

Therefore:

$$P\cdot\left([Ab]_{plasma} - [Ab]_{\text{int}}\right) = \frac{k_e\,[Ag]_0 \big/ \varepsilon}{S \big/ V}$$

$$[Ab]_{\text{int}} = [Ab]_{plasma} - \left(\frac{k_e\,[Ag]_0 \big/ \varepsilon}{P}\right)\cdot\left(\frac{V}{S}\right)$$

where $[Ab]_{\text{int}} = [Ab]_{cap}/\varepsilon$

Using cylindrical geometry as was used for the clearance modulus, the volume to surface area is:

$$\frac{V}{S} = \frac{A\cdot L}{C_i\cdot L} = \frac{A}{2\pi R_{cap}} = \frac{\pi(R_{sat}{}^2 - R_{cap}{}^2)}{2\pi R_{cap}} = \frac{R_{sat}{}^2 - R_{cap}{}^2}{2R_{cap}} \approx \frac{R_{sat}{}^2}{2R_{cap}}$$

where A is the area of saturation viewing the vessels on axis, L is the length along the vessel, C_i is the circumference of the vessel, R_{cap} is the capillary radius, and R_{sat} is the radius of saturated tissue surrounding the vessel. Generally, $R_{sat} >> R_{cap}$ justifying the last simplification. A hexagonal (array) geometry can be assumed, but this decreases the volume by less than 20%. ($A_{hexagon}/A_{circle} > 0.8$)

Combining:

$$P\cdot\left([Ab]_{plasma} - [Ab]_{\text{int}}\right) = \frac{k_e R_{sat}{}^2\left([Ag]_0 \big/ \varepsilon\right)}{2R_{cap}}$$

This is very close to our final definition for the Thiele modulus, derived from a simple mass balance. If we assume $[Ab]_{\text{int}} << [Ab]_{plasma}$, the remaining terms can be brought to the RHS, and this dimensionless group would be a defined parameter for quantifying catabolism.

$$1 = \frac{k_e R_{sat}{}^2\left([Ag]_0 \big/ \varepsilon\right)}{2PR_{cap}[Ab]_{plasma}}$$

$$\text{Scaling Parameter} = \frac{k_e R^2\left([Ag]_0 \big/ \varepsilon\right)}{2PR_{cap}[Ab]_{plasma}}$$

This follows similar logic to the clearance modulus definition. There is no consideration for the diffusive driving force necessary to maintain saturation at a given radius, however. By making an assumption based on previous studies of reaction/diffusion problems, we can arrive at a more general result that includes analysis of the required concentration driving force.

General Thiele modulus:

For a more general parameter based on the well studied Thiele modulus, the definition from the previous section will be used in conjunction with the mass balance. Solving this equation for R_{sat}:

$$\phi_{sat}^{\ 2} = \frac{k_e R_{sat}^{\ 2} [Ag]_0 / \varepsilon}{D[Ab]_{\text{int}}}$$

$$R_{sat}^{\ 2} = \frac{\phi_{sat}^{\ 2} D[Ab]_{\text{int}}}{k_e [Ag]_0 / \varepsilon}$$

Combining the mass balance with the saturated Thiele modulus equation:

$$P \cdot \left([Ab]_{plasma} - [Ab]_{\text{int}}\right) = \frac{k_e R_{sat}^{\ 2} \left([Ag]_0 / \varepsilon\right)}{2R_{cap}} = \frac{k_e \dfrac{\phi_{sat}^{\ 2} D[Ab]_{\text{int}}}{k_e [Ag]_0 / \varepsilon} \left([Ag]_0 / \varepsilon\right)}{2R_{cap}}$$

$$P \cdot \left([Ab]_{plasma} - [Ab]_{\text{int}}\right) = \frac{\phi_{sat}^{\ 2} D[Ab]_{\text{int}}}{2R_{cap}}$$

At this point in the derivation, the $[Ab]_{int}$ appears on both sides of the equation. This results from this concentration being involved both in the concentration gradient across the capillary wall ('external mass transfer') and determination in the level of saturation within the tissue ('internal mass transfer'). It is completely analogous to the surface concentration in a catalyst pellet in traditional chemical engineering. Similarly, it is very difficult to measure directly.

Solving for $[Ab]_{int}$:

$$[Ab]_{\text{int}} = \frac{[Ab]_{plasma}}{\left(\dfrac{\phi_{sat}^{\ 2} D}{2PR_{cap}} + 1\right)}$$

$$[Ab]_{\text{int}} = \frac{[Ab]_{plasma}}{\left(\dfrac{\phi_{sat}^{\ 2}}{Bi} + 1\right)}$$

where $Bi \equiv \left(\dfrac{2 \cdot P \cdot R_{cap}}{D}\right)$ = (diffusion resistance) / (capillary resistance)

Assumption for Thiele modulus:

To arrive at a simple scaling parameter, a final assumption is made. Extensive work previously analyzing the Thiele modulus shows that as this parameter drops below 1, the catalyst (binding sites in this analysis) becomes saturated. When this value increases above 1, the system becomes mass transport limited, and not all the catalyst sites (antigen binding sites) are occupied(*29*). It is assumed that the Thiele modulus is equal to 1 for the saturated core.

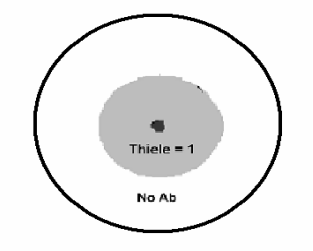

If the Thiele modulus value in the saturated core is larger than one, there will be transport limitations, antibody will not be able to diffuse to the edge of the core, and R_{sat} will decrease. If it is smaller than one, the system will be reaction limited, and extra antibody will diffuse beyond the small core, increasing R_{sat}. Under the shrinking core assumptions, the antibody turnover in the tissue is a zero-order reaction with a rate of $k_e[Ag]$. It was previously mentioned that the critical value of the Thiele modulus (where values less than this are saturated and values greater than this are not) for a sphere was $\sqrt{6}$. For the cylindrical case, it is a function of $R_{capillary}/R$, but the critical value for a 100 μm cylinder is ~1.1 with R_{cap} = 10 μm. Setting this value to 1, the transition point for entering the saturated regime, provides a direct relationship between $[Ab]_{int}$ and $[Ab]_{plasma}$. This assumption is not as restrictive as it may first appear because it affects the final definition of a scaling parameter, not an exact equality. Thus, it only has to be approximately one, and deviations will appear in the absolute value of the scaling parameter. This assumption, along with those previously, is then validated through full numerical simulations. This yields:

$$[Ab]_{\text{int}} = \frac{[Ab]_{plasma}}{\left(\frac{1}{Bi}+1\right)}$$

Using this value of the effective antibody concentration in the Thiele modulus:

$$\boxed{\phi^2 \equiv \frac{k_e R^2\left([Ag]_0 / \varepsilon\right)}{D\left(\frac{[Ab]_{plasma}}{1+1/Bi}\right)}}$$

For very small values of the Biot number, transport of the antibody to the tumor will be limited by the permeability, and a steep gradient will exist across the capillary wall. Thus, $[Ab]_{int}$ will be negligible compared to $[Ab]_{plasma}$. Plugging in the variables for the Biot number and simplifying for 1/Bi >> 1, the definition for the Thiele modulus becomes:

$$\phi^2 = \frac{k_e R^2\left([Ag]_0 / \varepsilon\right)}{2PR_{cap}[Ab]_{plasma}}$$

Thus, the general Thiele modulus simplifies to the scaling parameter in the previous section based on the mass balance alone.

For very large values of the Biot number, transport is only limited by diffusion. The concentration on the outside of the capillary will be equal to the plasma concentration. Simplifying the Thiele modulus for 1/Bi << 1 yields:

$$\phi^2 = \frac{k_e R^2 \left([Ag]_0 / \varepsilon \right)}{D[Ab]_{plasma}}$$

Thus, the general Thiele modulus takes the form of the original definition with $[Ab]_{int}=[Ab]_{plasma}$ when the gradient across the capillary is negligible.

F. Derivation of Clearance Modulus for Micrometastases

The saturation time for micrometastases is given in Graff et al.(5) To derive the AUC for metastases imbedded in normal tissue, the antibody concentration in normal tissue as a function of time is calculated from a two-compartment model:

$[Ab]_{plasma}(t) = [Ab]_{plasma,0}\left(Ae^{-k_1 t} + Be^{-k_2 t}\right)$ initial condition: $[Ab]_{plasma}(0) = [Ab]_{plasma,\,0}$

$\frac{d[Ab]_n}{dt} = \kappa[Ab]_{plasma}(t) - \lambda[Ab]_n(t)$ initial condition: $[Ab]_n(0) = [Ab]_{n0}$

$$[Ab]_n(t) = [Ab]_{plasma,0}\left(\mathrm{K}\left(\frac{Ae^{-k_1 t}}{\lambda - k_1} + \frac{Be^{-k_2 t}}{\lambda - k_2}\right) - \mathrm{K}\left(\frac{A}{\lambda - k_1} + \frac{B}{\lambda - k_2}\right)e^{-\lambda t}\right) + Ab_{n0}e^{-\lambda t}$$

Integrating from 0 to infinity:

$$\int_{t=0}^{t=\infty} Ab_n(t)dt = AUC = \int_{t=0}^{t=\infty}\left[[Ab]_{plasma,0}\left(\mathrm{K}\left(\frac{Ae^{-k_1 t}}{\lambda - k_1} + \frac{Be^{-k_2 t}}{\lambda - k_2}\right) - \mathrm{K}\left(\frac{A}{\lambda - k_1} + \frac{B}{\lambda - k_2}\right)e^{-\lambda t}\right) + Ab_{n0}e^{-\lambda t}\right]dt$$

$$AUC = [Ab]_{plasma,0}\,\mathrm{K}\left(\frac{Ae^{-k_1 t}}{-k_1(\lambda - k_1)} + \frac{Be^{-k_2 t}}{-k_2(\lambda - k_2)}\right)\Bigg|_{t=0}^{t=\infty} - [Ab]_{plasma,0}\,\mathrm{K}\left(\frac{A}{\lambda - k_1} + \frac{B}{\lambda - k_2}\right)\frac{e^{-\lambda t}}{-\lambda}\Bigg|_{t=0}^{t=\infty} + \frac{Ab_{n0}}{-\lambda}e^{-\lambda t}\Big|_{t=0}^{t=\infty}$$

$$AUC = [Ab]_{plasma,0}\,\mathrm{K}\left(\frac{A}{k_1(\lambda - k_1)} + \frac{B}{k_2(\lambda - k_2)}\right) - [Ab]_{plasma,0}\,\mathrm{K}\left(\frac{A}{\lambda - k_1} + \frac{B}{\lambda - k_2}\right)\frac{1}{\lambda} + \frac{Ab_{n0}}{\lambda}$$

$$\boxed{AUC = \frac{[Ab]_{n0}}{\lambda} + [Ab]_{plasma,0}\left(\frac{\mathrm{K}}{\lambda}\right)\left[\frac{A}{k_1} + \frac{B}{k_2}\right]}$$

G. Effective Internalization Constants

Using a compartmental model for internalization:

$$Surface \underset{k_{recycle}}{\overset{k_{internalization}}{\leftrightarrow}} Internal \overset{k_{degradation}}{\rightarrow} Degraded$$

I = internal concentration, S = surface concentration, and D = degraded concentration

$$\frac{dI}{dt} = k_i[S] - k_r[I] - k_d[I]$$

$$\frac{dD}{dt} = k_d[I]$$

Using a pseudo-steady state approximation where $\frac{dI}{dt} = 0$

$$\frac{dD}{dt} = \frac{k_i k_d}{k_r + k_d}[S]$$

This gives an 'effective' internalization rate $k_e = \frac{k_i k_d}{k_r + k_d}$ from

$$\frac{dD}{dt} = k_{effective}[S]$$

$$k_e = \frac{k_i k_d}{k_r + k_d} = \frac{k_i}{\left(\frac{k_r}{k_d}\right) + 1}$$

For Herceptin, 85% recycled and 15% degraded for each pass (*44*), so:

$$k_e = \frac{k_{\text{int}\,ernalization}}{\left(0.85 \diagup 0.15\right) + 1} = \frac{k_{\text{int}\,ernalization}}{6.7}$$

$$k_e = (0.15)k_{\text{int}\,ernalization} = 0.15 \cdot 2.2x10^{-4}\ /\ s = 3.3x10^{-5}\ /\ s$$

Or:

$$t_{1/2,e} = \frac{6.7 \cdot \ln(2)}{k_{\text{int}\,ernalization}} = 6.7 \cdot t_{1/2,\text{int}\,ernalization}$$

H. List of Symbols

The following symbols apply to the supplemental material unless redefined for a specific section.

A = fraction (0-1) of alpha phase clearance
[Ab] = Free antibody concentration
$[Ab]_{cap}$ = Antibody concentration on the abluminal side of the capillary using overall tissue volume
$[Ab]_{int}$ = Interstitial antibody concentration on abluminal side of capillary or surface of micrometastasis (using interstitial volume) = $[Ab]_{cap} / \varepsilon$
$[Ab]_n$ = Normal tissue compartment antibody concentration (for micrometastases)
$[Ab]_{n0}$ = Initial antibody concentration in normal tissue compartment
$[Ab]_{plasma}$ = Concentration of free antibody in blood plasma
$[Ab]_{plasma,0}$ = Initial concentration of free antibody in blood plasma
[Ag] or $[Ag]_t$ = Antigen concentration per total tumor volume
$[Ag]_0$ = Initial antigen concentration per total tumor volume
AUC = area under curve, used for the integral of plasma concentration over time
[B] = concentration of bound antibody-antigen complex using total tissue volume
B = fraction (0-1) of beta phase clearance
Bi = mass transfer Biot number, the ratio of capillary transport to diffusive transport
D = (effective) diffusion coefficient
ε = effective void fraction (antibody accessible volume / total volume) – e.g. 0.5 for small molecule (salts), 0.3 for scFv, and 0.1 for IgG
Γ_{met} = clearance modulus defined for metastasis
Γ_{tumor} = clearance modulus defined for solid tumor
∇ = gradient operator
∇^2 = Laplacian
k_α = alpha phase clearance rate constant = $\ln(2)/t_{1/2,\alpha}$
k_β = beta phase clearance rate constant = = $\ln(2)/t_{1/2,\beta}$
k_e = endocytosis rate constant
k_r = recycle rate constant
k_d = degradation rate constant
k_i = internalization rate constant
K_d = equilibrium dissociation constant
k_{on} = antibody binding rate constant
k_{off} = antibody dissociation rate constant
P = capillary permeability
r = radius
R = radius of reacting front/radius of saturation in shrinking core derivation or an arbitrary radius of interest as used in the clearance and Thiele modulus
R_{cap} = capillary radius
R_{max} = the maximum radius that would be saturated under the given conditions
R_s = antigen synthesis rate
R_{sat} = radius of reacting front/saturation radius in Thiele modulus derivation
t = time
$t_{1/2}$ = half life
$t_{infusion}$ = length of time for constant infusion/constant blood plasma concentration
t_{sat} = saturation time
ϕ_{met} = Thiele modulus defined for metastasis
ϕ_{sat} = value of Thiele modulus at which point saturation occurs
ϕ_{tumor} = Thiele modulus defined for solid tumor

SUPPLEMENTAL REFERENCES

1. National Cancer Institute Clinical Trials. web site] www.cancer.gov/clinicaltrials.

2. *Medicines in Development for Biotechnology*: Pharmaceutical Research and Manufacturers of America; 2004.

3. Weinstein J, Eger R, Covell D, et al. The Pharmacology of Monoclonal Antibodies. *Annals New York Academy of Sciences.* 1987;507:199-210.

4. Jain RK. Transport of Molecules, Particles, and Cells in Solid Tumors. *Annual Reviews in Biomedical Engineering.* 1999;01:241-263.

5. Graff C, Wittrup KD. Theoretical Analysis of Antibody Targeting of Tumor Spheroids: Importance of Dosage for Penetration, and Affinity for Retention. *Cancer Research.* 2003;63:1288-1296.

6. Kyriakos R, Shih L, Ong G, Patel K, Goldenberg D, Mattes MJ. The Fate of Antibodies Bound to the Surface of Tumor Cells *in Vitro*. *Cancer Research.* 1992;52:835-842.

7. Mattes MJ, Griffiths G, Diril H, Goldenberg D, Ong G, Shih L. Processing of Antibody-Radioisotope Conjugates after Binding to the Surface of Tumor Cells. *Cancer.* 1994;73:787-793.

8. Maxfield F, McGraw T. Endocytic Recycling. *Nature Reviews Molecular Cell Biology.* 2004;5:121-132.

9. Gerlowski L, Jain RK. Microvascular Permeability of Normal and Neoplastic Tissues. *Microvascular Research.* 1986;31:288-305.

10. Baxter L, Jain RK. Transport of Fluid and Macromolecules in Tumors 1. Role of Interstitial Pressure and Convection. *Microvascular Research.* 1989;37:77-104.

11. Casalini P, Luison E, Menard S, Colnaghi M, Paganelli G, Canevari S. Tumor Pretargeting: Role of Avidin/Streptavidin on Monoclonal Antibody Internalization. *The Journal of Nuclear Medicine.* 1997;38(9):1378-1381.

12. Chan MC, Murphy RM. Kinetics of cellular trafficking and cytotoxicity of 9.2.27-gelonin immunotoxins targeted against the high-molecular-weight melanoma-associated antigen. *Cancer Immunol Immunother.* Feb 1999;47(6):321-329.

13. Ford C, Tsaltas G, Osbourne P, Addetia K. Novel Flow Cytometric Analysis of the Progress and Route of Internalization of a Monoclonal Anti-Carcinoembryonic Antigen (CEA) Antibody. *Cytometry.* 1996;23:228-240.

14. Mariani G, D A, Venkateshan C, et al. Monoclonal Antibody Internalization by Tumor Cells: an Experimental Model for Potential Radioimmunotherapy Applications. *Nuclear Medicine and Biology.* 1989;16(2):147-150.

15. Matzku S, Brocker E, Bruggen J, Dippold W, Tilgen W. Modes of Binding and Internalization of Monoclonal Antibodies to Human Melanoma Cell Lines. *Cancer Research.* 1986;46:3848-3854.

16. Schaffar L, Dallanegra A, Breittmayer J, Carrel S, Fehlmann M. Monoclonal Antibody Internalization and Degradation during Modulation of the CD3/T-Cell Receptor Complex. *Cellular Immunology.* 1988;116:52-59.

17. Tsaltas G, Ford C, Gallant M. Demonstration of Monoclonal Anti-Carcinoembryonic Antigen (CEA) Antibody Internalization by Electron Microscopy, Western Blotting and Radioimmunoassay. *Anticancer Research.* 1992;12:2133-2142.

18. Wenning LA, Murphy RM. Coupled cellular trafficking and diffusional limitations in delivery of immunotoxins to multicell tumor spheroids. *Biotechnology and Bioengineering.* Mar 5 1999;62(5):562-575.

19. Rippley RK, Stokes CL. Effects of Cellular Pharmacology on Drug Distribution in Tissues. *Biophysical Journal.* Sep 1995;69(3):825-839.

20. Adams G, Schier R, McCall A, et al. High Affinity Restricts the Localization and Tumor Penetration of Single-Chain Fv Antibody Molecules. *Cancer Research.* 2001;61:4750-4755.

21. Hjelstuen MH, Rasch-Halvorsen K, Bruland O, Davies CD. Uptake, penetration, and binding of monoclonal antibodies with increasing affinity in human osteosarcoma multicell spheroids. *Anticancer Research.* Sep-Oct 1998;18(5A):3153-3161.

22. Baish J, Gazit Y, Berk D, Nozue M, Baxter L, Jain RK. Role of Tumor Vascular Architecture in Nutrient and Drug Delivery: An Invasion Percolation-Based Network Model. *Microvascular Research.* 1996;51:327-346.

23. Sutherland R. Cell and Environment Interactions in Tumor Microregions: The Multicell Spheroid Model. *Science.* 1988;240:177-184.

24. Pluen A, Boucher Y, Ramanujan S, et al. Role of tumor-host interactions in interstitial diffusion of macromolecules: Cranial vs. subcutaneous tumors. *Proceedings of the National Academy of Sciences of the United States of America.* Apr 10 2001;98(8):4628-4633.

25. Behr T, Becker W, Hannappel E, Goldenberg D, Wolf F. Targeting of Liver Metastases of Colorectal Cancer with IgG, $F(ab')_2$, and Fab' Anti-Carcinoembryonic

Antigen Antibodies Labeled with ^{99m}Tc: The Role of Metabolism and Kinetics. *Cancer Research.* 1995;55:5777s-5785s.

26. Baxter LT, Jain RK. Transport of Fluid and Macromolecules in Tumors .4. A Microscopic Model of the Perivascular Distribution. *Microvascular Research.* Mar 1991;41(2):252-272.

27. Fujimori K, Covell D, Fletcher J, Weinstein J. Modeling Analysis of the Global and Microscopic Distribution of Immunoglobulin G, $F(ab')_2$, and Fab in Tumors. *Cancer Research.* 1989;49:5656-5663.

28. Ahlstrom H, Christofferson R, Lorelius L. Vascularization of the continuous human colonic cancer cell line LS 174 T deposited subcutaneously in nude rats. *APMIS.* 1988;96:701-710.

29. Aris R. *The mathematical theory of diffusion and reaction in permeable catalysts.* Vol I. Oxford: Clarendon Press; 1975.

30. Heicappell R, Muller-Mattheis V, Reinhardt M, et al. Staging of pelvic lymph nodes in neoplasms of the bladder and prostate by positron emission tomography with 2-F-18 -2-deoxy-D-glucose. *European Urology.* Dec 1999;36(6):582-587.

31. Kumar R, Alavi A. Clinical applications of fluorodeoxyglucose-positron emission tomography in the management of malignant melanoma. *Current Opinion in Oncology.* Mar 2005;17(2):154-159.

32. Saisho H, Yamaguchi T. Diagnostic imaging for pancreatic cancer - Computed tomography, magnetic resonance imaging, and positron emission tomography. *Pancreas.* Apr 2004;28(3):273-278.

33. Willkomm P, Bender H, Bangard M, Decker P, Grunwald F, Biersack H. FDG PET and Immunoscintigraphy with ^{99m}Tc-Labeled Antibody Fragments for Detection of the Recurrence of Colorectal Carcinoma. *The Journal of Nuclear Medicine.* 2000;41(10):1657-1663.

34. Friedman LM, Rinon A, Schechter B, et al. Synergistic down-regulation of receptor tyrosine kinases by combinations of mAbs: Implications for cancer immunotherapy. *Proceedings of the National Academy of Sciences of the United States of America.* Feb 8 2005;102(6):1915-1920.

35. Hendriks BS, Opresko LK, Wiley HS, Lauffenburger D. Coregulation of epidermal growth factor receptor/human epidermal growth factor receptor 2 (HER2) levels and locations: Quantitative analysis of HER2 overexpression effects. *Cancer Research.* Mar 1 2003;63(5):1130-1137.

36. Rao BM, Lauffenburger DA, Wittrup KD. Integrating cell-level kinetic modeling into the design of engineered protein therapeutics. *Nature Biotechnology.* Feb 2005;23(2):191-194.

37. Chaplin DJ, Olive PL, Durand RE. Intermittent Blood-Flow in a Murine Tumor - Radiobiological Effects. *Cancer Research.* Jan 15 1987;47(2):597-601.

38. Eskey CJ, Koretsky AP, Domach MM, Jain RK. H-2-Nuclear Magnetic-Resonance-Imaging of Tumor Blood-Flow - Spatial and Temporal Heterogeneity in a Tissue-Isolated Mammary Adenocarcinoma. *Cancer Research.* Nov 1 1992;52(21):6010-6019.

39. Kaminski MS, Zasadny KR, Francis IR, et al. Radioimmunotherapy of B-Cell Lymphoma with I-131 Anti-B1 (Anti-Cd20) Antibody. *New England Journal of Medicine.* Aug 12 1993;329(7):459-465.

40. Wiseman GA, White CA, Stabin M, et al. Phase I/II Y-90-Zevalin (yttrium-90 ibritumomab tiuxetan, IDEC-Y2B8) radioimmunotherapy dosimetry results in relapsed or refractory non-Hodgkin's lymphoma. *European Journal of Nuclear Medicine.* Jul 2000;27(7):766-777.

41. Tong R, Boucher Y, Kozin S, Winkler F, Hicklin D, Jain RK. Vascular Normalization by Vascular Endothelial Growth Factor Receptor 2 Blockade Induces a Pressure Gradient Across the Vasculature and Improves Drug Penetration in Tumors. *Cancer Research.* 2004;64:3731-3736.

42. Baxter L, Jain RK. Transport of Fluid and Macromolecules in Tumors: 3. Role of Binding and Metabolism. *Microvascular Research.* 1991;41:5-23.

43. Thiele EW. Relation between Catalytic Activity and Size of Particle. *Industrial and Engineering Chemistry.* 1939;31(7):916-920.

44. Austin C, Maziere A, Pisacane P, et al. Endocytosis and Sorting of ErbB2 and the Site of Action of Cancer Therapeutics Trastuzumab and Geldanamycin. *Molecular Biology of the Cell.* 2004;15:5268-5282.

45. Thilo L. Quantification of endocytosis-derived membrane traffic. *Biochimica et Biophysica Acta.* 1985;822:243-266.

46. Nichols B, Kenworthy A, Polishchuk R, et al. Rapid Cycling of Lipid Raft Markers between the Cell Surface and Golgi Complex. *Journal of Cell Biology.* 2001;153(3):529-541.

47. Brown E, Boucher Y, Nasser S, Jain RK. Measurement of macromolecular diffusion coefficients in human tumors. *Microvascular Research.* 2004;67:231-236.

48. Praxmarer M, Sung C, Bungay PM, van Osdol WW. Computational models of antibody-based tumor imaging and treatment protocols. *Annals of Biomedical Engineering.* Apr 2001;29(4):340-358.

49. Fujimori K, Covell D, Fletcher J, Weinstein J. A Modeling Analysis of Monoclonal Antibody Percolation Through Tumors: A Binding-Site Barrier. *The Journal of Nuclear Medicine.* 1990;31:1191-1198.

50. Boucher Y, Pluen A, Ramanujan S, McKee T, Jain RK. INTERSTITIAL DIFFUSION OF MACROMOLECULES IN SOLID TUMORS: ROLE OF THE INTERSTITIAL MATRIX. Paper presented at: Bioengineering Conference ASME, 2001.

51. McIntosh D, Tan X, Oh P, Schnitzer J. Targeting endothelium and its dynamic caveolae for tissue-specific transcytosis *in vivo*: A pathway to overcome cell barriers to drug and gene delivery. *Proceedings of the National Academy of Science, USA.* 2002;99(4):1996-2001.

52. Vogel SM, Minshall RD, Pilipovic M, Tiruppathi C, Malik AB. Albumin uptake and transcytosis in endothelial cells in vivo induced by albumin-binding protein. *American Journal of Physiology-Lung Cellular and Molecular Physiology.* Dec 2001;281(6):L1512-L1522.

53. Baselga J, Norton L, Albanell J, Kim YM, Mendelsohn J. Recombinant humanized anti-HER2 antibody (Herceptin (TM)) enhances the antitumor activity of paclitaxel and doxorubicin against HER2/neu overexpressing human breast cancer xenografts. *Cancer Research.* 1998;58(13):2825-2831.

54. Hudziak R, Lewis G, Winget M, Fendly B, Shepard M, Ullrich A. $p185^{HER2}$ Monoclonal Antibody Has Antiproliferative Effects In Vitro and Sensitizes Human Breast Tumor Cells to Tumor Necrosis Factor. *Molecular and Cellular Biology.* 1989;9(3):1165-1172.

55. Clynes RA, Towers TL, Presta LG, Ravetch JV. Inhibitory Fc receptors modulate in vivo cytoxicity against tumor targets. *Nature Medicine.* Apr 2000;6(4):443-446.

56. Jain RK. Normalization of tumor vasculature: An emerging concept in antiangiogenic therapy. *Science.* Jan 7 2005;307(5706):58-62.

57. Tokuda Y, Ohnishi Y, Shimamura K, et al. In vitro and in vivo anti-tumour effects of a humanised monoclonal antibody against c-erbB-2 product. *British Journal of Cancer.* Jun 1996;73(11):1362-1365.

58. Lustig HJ, Bianco C. Antibody-Mediated Cell Cytotoxicity in a Defined System - Regulation by Antigen, Antibody, and Complement. *Journal of Immunology.* 1976;116(1):253-260.

59. Fenwick J, Philpott G, Connett J. Biodistribution and histological localization of anti-human colon cancer monoclonal antibody (MAb) 1A3: the influence of administered MAb dose on tumor uptake. *International Journal of Cancer.* 1989;44:1017-1027.

60. Liu GZ, He J, Dou SP, Gupta S, Rusckowski M, Hnatowich DJ. Further investigations of morpholino pretargeting in mice - establishing quantitative relations in tumor. *European Journal of Nuclear Medicine and Molecular Imaging.* Sep 2005;32(9):1115-1123.

61. Kranenborg M, Boerman OC, Oosterwijk-Wakka JC, De Weijert MCA, Corstens FHM, Oosrterwijk E. Two-step radio-immunotargeting of renal-cell carcinoma xenografts in nude mice with anti-renal-cell-carcinoma X anti-DTPA bispecific monoclonal antibodies. *International Journal of Cancer.* Jan 5 1998;75(1):74-80.

62. Sharkey RM, Karacay H, Richel H, et al. Optimizing bispecific antibody pretargeting for use in radioimmunotherapy. *Clinical Cancer Research.* Sep 1 2003;9(10):3897S-3913S.

63. Koppe E, Soede AC, Pels W, et al. Experimental radioimmunotherapy of small peritoneal metastases of colorectal origin. *International Journal of Cancer.* Oct 10 2003;106(6):965-972.

64. Yao ZS, Zhang ML, Axworthy DB, et al. Radioimmunotherapy of A431 xenografted mice with pretargeted B3 antibody-streptavidin and Y-90-labeled 1,4,7,10-tetraazacyclododecane-N,N ',N ",N "'-tetraacetic acid (DOTA)-biotin. *Cancer Research.* Oct 15 2002;62(20):5755-5760.

65. Begent RHJ, Verhaar MJ, Chester KA, et al. Clinical evidence of efficient tumor targeting based on single-chain Fv antibody selected from a combinatorial library. *Nature Medicine.* Sep 1996;2(9):979-984.

66. Wu A, Williams L, Zieran L, et al. Anti-carcinoembryonic antigen (CEA) diabody for rapid tumor targeting and imaging. *Tumor Targeting.* 1999;4:47-58.

67. Noguchi Y, Wu J, Duncan R, et al. Early phase tumor accumulation of macromolecules: a great difference in clearance rate between tumor and normal tissues. *Japanese Journal of Cancer Research.* Mar 1998;89(3):307-314.

68. *CEA-Scan, Arcitumomab Package Insert*.

69. Behr TM, Behe M, Stabin MG, et al. High-linear energy transfer (LET) alpha versus low-LET beta emitters in radioimmunotherapy of solid tumors: Therapeutic efficacy and dose-limiting toxicity of Bi-213- versus Y-90-labeled CO17-1A Fab ' fragments in a human colonic cancer model. *Cancer Research.* Jun 1 1999;59(11):2635-2643.

70. Baselga J, Carbonell X, Castaneda-Soto NJ, et al. Phase II study of efficacy, safety, and pharmacokinetics of trastuzumab monotherapy administered on a 3-weekly schedule. *Journal of Clinical Oncology.* 2005;23(10):2162-2171.

71. Ghetie V, Popov S, Borvak J, et al. Increasing the serum persistence of an IgG fragment by random mutagenesis. *Nature Biotechnology.* Jul 1997;15(7):637-640.

72. Mayor S, Rothberg K, Maxfield F. Sequestration of GPI-Anchored Proteins in Caveolae Triggered by Cross-Linking. *Science.* 1994;264(5167):1948-1951.

73. Niwa R, Sakurada M, Kobayashi Y, et al. Enhanced natural killer cell binding and activation by low-fucose IgG1 antibody results in potent antibody-dependent cellular cytotoxicity induction at lower antigen density. *Clinical Cancer Research.* Mar 15 2005;11(6):2327-2336.

74. Schoeberl B, Eichler-Jonsson C, Gilles ED, Muller G. Computational modeling of the dynamics of the MAP kinase cascade activated by surface and internalized EGF receptors. *Nature Biotechnology.* Apr 2002;20(4):370-375.

75. Alexandrakis G, Brown E, Tong R, et al. Two-photon fluorescence correlation microscopy reveals the two-phase nature of transport in tumors. *Nature Medicine.* 2004;10(2):203-207.

76. Hilmas D, Gillette E. MORPHOMETRIC ANALYSES OF THE MICROVASCULATURE OF TUMORS DURING GROWTH AND AFTER X-IRRADIATION. *Cancer.* 1974;33:103-110.

77. Yuan F, Dellian M, Fukumura D, et al. Vascular Permeability in a Human Tumor Xenograft: Molecular Size Dependence and Cutoff Size. *Cancer Research.* 1995;55:3752-3756.

78. Lyng H, Haraldseth O, Rofstad EK. Measurement of cell density and necrotic fraction in human melanoma xenografts by diffusion weighted magnetic resonance imaging. *Magnetic Resonance in Medicine.* Jun 2000;43(6):828-836.

79. Krol A, Nagaraj S, Dewhirst M, Yuan F. Available volume fraction of macromolecules in tumor tissues. *Faseb Journal.* Mar 15 2000;14(4):A167-A167.

80. Worthylake R, Opresko LK, Wiley HS. ErbB-2 amplification inhibits down-regulation and induces constitutive activation of both ErbB-2 and epidermal growth factor receptors. *Journal of Biological Chemistry.* Mar 26 1999;274(13):8865-8874.

81. Berk D, Yuan F, Leunig M, Jain RK. Direct *in vivo* measurement of targeted binding in a human tumor xenograft. *Proceedings of the National Academy of Science, USA.* 1997;94:1785-1790.

82. Schier R, McCall A, Adams GP, et al. Isolation of picomolar affinity Anti-c-erbB-2 single-chain Fv by molecular evolution of the complementarity determining regions in the center of the antibody binding site. *Journal of Molecular Biology.* Nov 8 1996;263(4):551-567.

83. Larson SM, Brown JP, Wright PW, Carrasquillo JA, Hellstrom I, Hellstrom KE. Imaging of Melanoma with I-131-Labeled Monoclonal-Antibodies. *Journal of Nuclear Medicine.* 1983;24(2):123-129.

84. Lin YS, Nguyen C, Mendoza JL, et al. Preclinical pharmacokinetics, interspecies scaling, and tissue distribution of a humanized monoclonal antibody against vascular endothelial growth factor. *Journal of Pharmacology and Experimental Therapeutics.* Jan 1999;288(1):371-378.

85. Scott AM, Lee FT, Jones R, et al. A phase I trial of humanized monoclonal antibody A33 in patients with colorectal carcinoma: Biodistribution, pharmacokinetics, and quantitative tumor uptake. *Clinical Cancer Research.* Jul 1 2005;11(13):4810-4817.

86. Milenic DE, Yokota T, Filpula DR, et al. Construction, Binding-Properties, Metabolism, and Tumor Targeting of a Single-Chain Fv Derived from the Pancarcinoma Monoclonal-Antibody Cc49. *Cancer Research.* Dec 1 1991;51(23):6363-6371.